Utrecht University

Faculty of Science

Theoretical models of a liquid crystal of banana-shaped colloidal particles

Master Thesis

Salma Ismaili BSc

Theoretical Physics

Supervisors:

Prof. dr. René van Roij

Institute for Theoretical Physics, Utrecht

Prof. dr. Bela Mulder

Institute for Theoretical Physics, Utrecht

Prof. dr. ir. Marjolein Dijkstra

Debye Institute for Nanomaterials Science, Utrecht

9th July 2022

Abstract

Since the discovery of liquid crystals in 1888 and the first theoretical models in the late 1940s, the interest in liquid crystals of particles of all different shapes and sizes has only increased. In addition to the nematic and smectic phases observed in liquid crystals of hard rods, liquid crystals of banana-shaped particles were observed to exhibit additional phases such as the twist-bend and splay-bend phase. In this thesis, two different theoretical models to describe a liquid crystal of banana-shaped particles are studied. Landau-de Gennes theory is shown to be able to describe the twist-bend and splay-bend phases, but has some drawbacks due to its phenomenological nature. Density functional theory in combination with bifurcation analysis is then proposed as an alternative approach that is based on the microscopic details of the particles, which are encoded in the excluded volume. With the use of symmetry arguments, a basis of the excluded volume of two banana-shaped particles in terms of symmetry-adapted functions is constructed. This microscopic approach opens up many opportunities for describing the complicated phases and phase transitions of liquid crystals of anisotropically-shaped particles.

Acknowledgements

With this master's thesis, my time at Utrecht University and the Institute for Theoretical Physics has come to an end. I am extremely grateful to my supervisor René van Roij for his immense support and valuable feedback. His enthusiasm and positive attitude kept me motivated at times when I felt discouraged, and the intuitive way in which he approaches new problems has inspired me on many occasions.

Writing this thesis would have not been possible without the guidance of Bela Mulder. The extensive knowledge and insights that he shared with me during our Zoom calls were a valuable contribution to this work. I would like to thank Marjolein Dijkstra for always asking the right questions and being involved in my project. I also had the pleasure of working with Rodolfo Subert and Gerardo Campos Villalobos and would like to thank them for their input and calculations.

I would like to thank Thijs, Tim K., Floris, Sebastian, Tim V., Willem, Alexander and Haolan, for their helpful feedback on my presentations and the fun group meetings. Special thanks to my fellow students Justus, Olaf, Margot, Iris, Franca, Casper, Lucas, Mithuss, Bianca and many others. Their support during the past six years has made my time at the university so much more enjoyable. Lastly, I would like to thank my parents for always checking up on me and believing in me, and Ravi for all the cooked dinners, solved Mathematica problems and endless moral support, for which I am very grateful.

Contents

Introduction

The story of liquid crystals started in 1888 [1, 2], when an Austrian botanist Friedrich Reinitzer studied cholesteryl benzoate found in carrots. He observed two melting points: the first time the compound melted it turned cloudy, before melting again into a clear liquid. The German physicist that Friedrich had asked for help, Otto Lehman, studied the cloudy fluid under a microscope. He noticed that the compound flowed like a fluid but had an ordered molecular structure, which was more characteristic of a solid. He concluded that this cloudy fluid must be in a new state of matter and called it a liquid crystal.

At first, the idea of a liquid crystal might sound absurd. How can something be a liquid and a crystal at the same time? However, it should be seen more as an intermediate state with characteristics from both phases. A liquid crystal possesses typical properties of a liquid, like fluidity, the inability to resist shearing stress and the ability to form droplets. It also shows some crystalline properties, such as ordering of the particles in one or more directions and anisotropy in optical, electrical and magnetic properties.

After the first discovery in 1888, science was not ready to accept this new and seemingly absurd concept, even though a number of experiments in the years later confirmed the existence of liquid crystals. It wasn't until the 1960s when the French physicist Pierre-Gilles de Gennes developed a theoretical model of the properties of liquid crystals [3]. His research on liquid crystals was part of the reason why he received the 1991 Nobel Prize in Physics. There was however an other physicist, Lars Onsager, that laid the ground work for a theory of liquids a few decades earlier. In 1949, Onsager predicted that fluids of hard rods undergo a phase transition from an isotropic phase to a nematic phase where the particles exhibit global orientational ordering, based purely on repulsive intermolecular forces [4].

Soon after, the first liquid-crystal display (LCD) products were announced in 1969, including animated advertisements and a rear-view mirror with reduced glare. Nowadays, liquid crystals can be found in displays of televisions, clocks and phones, as well as in liquid crystal thermometers, optical filters and liquid crystal lenses. The increased interest in liquid crystals has also encouraged new experimental, theoretical, and computational studies of liquid crystals of particles with more exotic shapes. Recently, a liquid crystal of hard banana-shaped colloidal particles was found to exhibit new and exciting phases such as the twist-bend, the splay-bend, and the intermediate twist-splay-bend phases [5, 6].

In this thesis I will present two different theoretical models to describe these new phases of a liquid crystal of banana-shaped particles and its phase transitions. After introducing liquid crystals in Chapter 1, I will discuss the characteristics and phases of a liquid crystal of banana-shaped particles, including some computational and experimental findings in Chapter 2. In Chapter 3, I will introduce Landau-de Gennes theory, which is a powerful theory based on the Landau theory of phase transitions. After discussing the drawbacks of Landau-de Gennes theory, a more promising alternative is proposed in Chapter 4, namely density functional theory which is based on the microscopic details of a liquid crystal. Following an introduction into point groups and representation theory in Chapter 5, I will show how the symmetries of the

constituting particles have a direct impact on the symmetries of the resulting liquid-crystal phases. In Chapter 6, I will describe three different approaches to a theoretical model of a liquid crystal of hard rods with restricted orientations. Finally, these ideas will be used to construct a theoretical description of a liquid crystal of banana-shaped particles with restricted orientations in Chapter 7.

CHAPTER 1

Liquid crystals

1.1 Introduction to liquid crystals

Molecules with a roughly spherical shape form three types of equilibrium phases: a gas, a liquid, and a solid (or crystal) phase. They differ in the degree of ordering of the particles. Gases and liquids have no translational or rotational order, but differ in density, while the particles in crystals are (almost) perfectly ordered on a densely-packed lattice. Systems with less symmetrical particles, i.e. particles that are elongated in one or more directions such as rods or discs, form additional phases [7]. These mesophases are called liquid crystals and have a degree of ordering in between that of liquids and crystals. Snapshots of the most common phases formed by rod-like particles, i.e. the crystalline, smectic, nematic, and isotropic phase, are schematically depicted in Fig. 1.1 with decreasing degree of ordering.

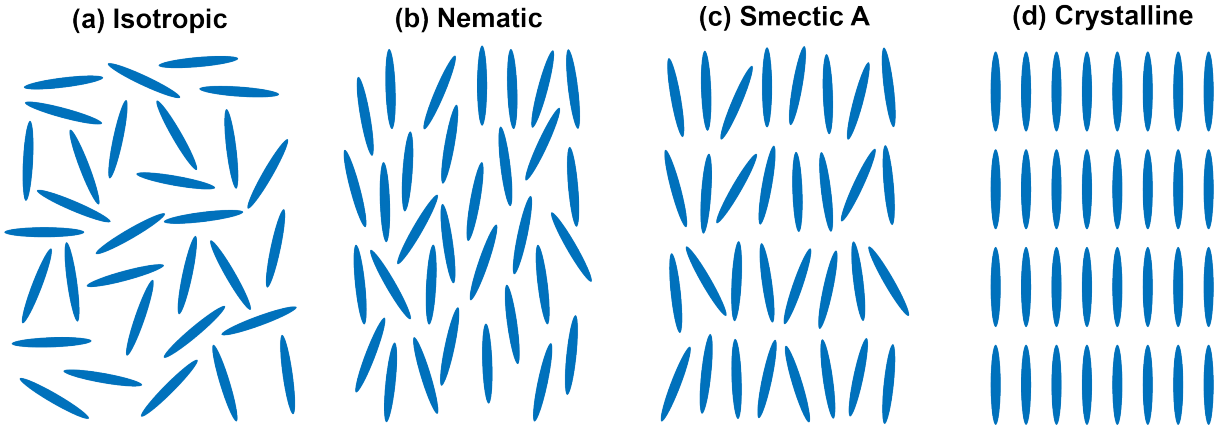

Figure 1.1: Different phases of a system with rod-like particles with increasing degree of ordering: (a) isotropic, (b) nematic, (c) smectic, and (d) crystalline.

Nematic liquid crystals

The simplest liquid crystal phase is the nematic phase [7, 8], which is characterised by long-range orientational order. In a bulk nematic liquid crystal, the particles are distributed homogeneously but their orientations are no longer isotropically distributed. The long body axis vectors $\boldsymbol{u}_i$ of the particles labeled by i are more or less aligned along a preferred axis known as the nematic director represented by the unit vector $\boldsymbol{n}$ (see Fig. 1.2). The isotropic symmetry of a gas or liquid is broken in the nematic phase. The bulk nematic phase has inversion and cylindrical symmetry, which means that the thermodynamics does not change by inverting the director $\boldsymbol{n} \to -\boldsymbol{n}$ or by rotating the particles along their main body axis.

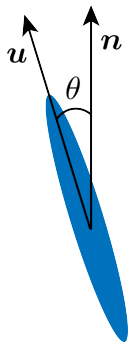

Figure 1.2: Schematic representation of a rod-like particle with main body axis $\boldsymbol{u}$ and nematic director $\boldsymbol{n}$ with θ the conical angle between $\boldsymbol{u}$ and $\boldsymbol{n}$.

Smectic liquid crystals

An other possible liquid crystal phase is called the smectic phase [7, 8], a phase in which the particles are arranged in layers and have translational order in one dimension in addition to orientational order. In the nematic-to-smectic phase transition, the system crystallizes in one direction and remains fluid-like in the other two directions. Several different smectic phases have been observed. In the smectic A phase, the molecules are aligned perpendicular to the layers. The smectic C phase is a biaxial phase where the nematic director is not perpendicular to the layers.

1.2 Oseen-Frank theory

Although liquid crystals flow like fluids, they resemble solids in the way they respond elastically to mechanical deformation of the director field $\boldsymbol{n}$. The simplest theory to describe these effects is the Oseen-Frank theory. According to this theory, the elastic energy due to an inhomogeneous director field $\boldsymbol{n}(\boldsymbol{r})$ is given by [9, 10]

$$E(\boldsymbol{n}) = \frac{1}{2}\int d\boldsymbol{r}\left[K_{11}(\nabla\cdot\boldsymbol{n}(\boldsymbol{r}))^2 + K_{22}(\boldsymbol{n}(\boldsymbol{r})\cdot\nabla\times\boldsymbol{n}(\boldsymbol{r}))^2 + K_{33}\left|\boldsymbol{n}(\boldsymbol{r})\times(\nabla\times\boldsymbol{n}(\boldsymbol{r}))^2\right|\right] \quad (1.1)$$

where K_{11}, K_{22}, and K_{33} are material-dependent elastic constants and correspond to the splay, twist and bend distortions as shown in Fig. 1.3. Sometimes a fourth term with elastic constant K_{24}, corresponding to the saddle-splay distortion, is included.

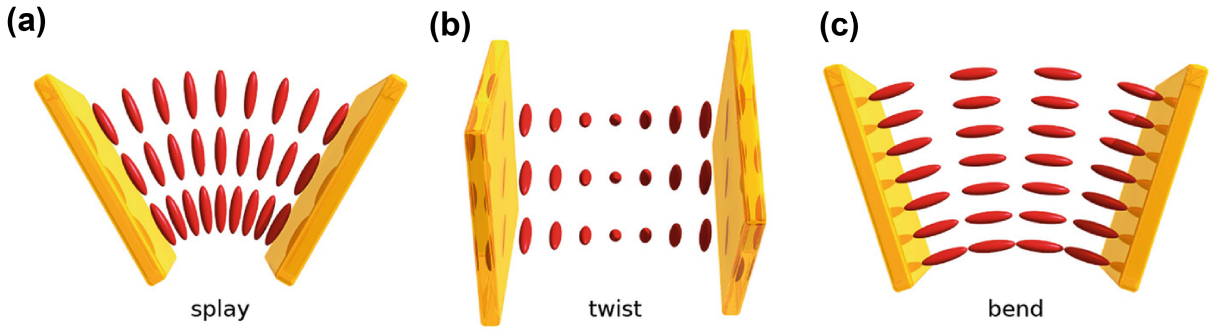

Figure 1.3: The three elastic modes in the Oseen-Frank theory: (a) splay, (b) twist, and (c) bend. Figure adapted from Ref. [11].

Because of its simplicity, Oseen-Frank theory fails to describe some of the features of nematic liquid crystals, such as the isotropic-to-nematic phase transition and the structure of defects. This is because Oseen-Frank-like models oversimplify the orientational properties by only considering a long-axis director field and writing the free energy in terms of its derivatives. Consequently, it does not succeed in describing orientational properties beyond the single main axis. In addition, it does not take into account the symmetry of the particles and has singularities at defect points. It is therefore not the most comprehensive theory to describe liquid crystals phases. An example of a theory that incorporates additional degrees of freedom is Landau-de Gennes theory, which will be discussed in Section 3.3.

1.3 Thermotropic versus lyotropic liquid crystals

Liquid crystal phase transitions occur either as a function of temperature for thermotropic liquid crystals [8], or as a function of density in the case of lyotropic liquid crystals [12]. Thermotropic nematics are one-component fluids of molecules. The phase transition from the isotropic to the nematic phase is driven by enthalpy. The attractive interactions have to compensate for the loss of orientational entropy upon alignment. Therefore, temperature is the relevant thermodynamic variable. As the temperature increases, the degree of ordering decreases.

Lyotropic nematics are rod- or plate-like particles finely dispersed in a host fluid. The particles are colloidal with a size of the order of 10 nanometers to a few microns, which makes them larger than molecules but smaller than what is visible with the human eye. This is the regime where Brownian motion due to collisions with the solvent molecules is possible and gravity is relatively weak ($k_BT \sim mgh$). This means that the principles of statistical physics can be applied to colloidal particles. The isotropic-to-nematic phase transition is driven by competition between translational entropy and orientational entropy. Since translational entropy depends on the free volume, the concentration or particle density is the relevant variable here. Liquid crystals of colloidal particles will be the focus of this thesis.

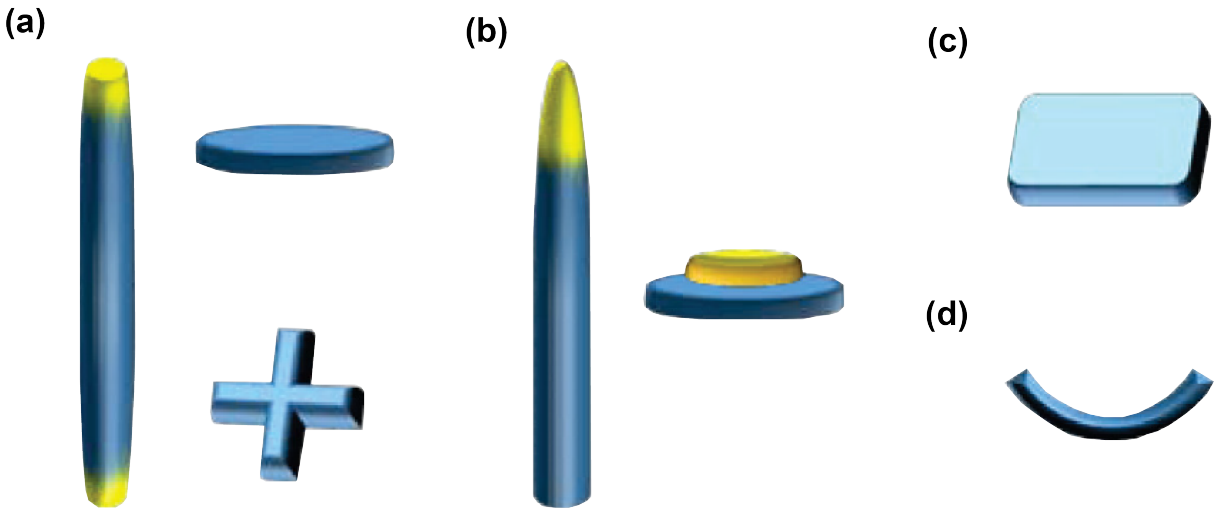

Figure 1.4: Examples of different particle shapes: (a) a rod, disc and cross with D_{4h} symmetry, (b) a polar rod and polar disc with C_{4v} symmetry, (c) a rectangular box with D_{2h} symmetry, and (d) a banana-shaped particle with C_{2v} symmetry. Figure adapted from Ref. [13].

1.4 Anisotropically-shaped particles

Next to rod-like and disk-like particles, there are particles with more exotic shapes. The particle symmetries are described by discrete point symmetry groups (see Chapter 5). For convenience, we restrict the orientations of the particles to have their body axes aligned with the coordinate frame axes in 3D.

In a model with restricted orientations, a rod, disk and cross all belong to the D_{4h} symmetry group. This point group can be described with one four-fold rotation axis C_4, one two-fold rotation axis C_2 with four two-fold rotation axes C_2 perpendicular to it, two vertical (σ_v), two diagonal (σ_d) and one horizontal (σ_h) mirror plane.

If one side of the rod or disk is different from the opposite side, the particles are called polar rods or polar disks and their symmetry is described by the C_{4v} point group. This symmetry group is equal to the D_{4h} symmetry group without the four perpendicular C_2 rotation axes and the horizontal mirror plane σ_h. Rectangular boxes or cuboids have symmetry group D_{2h} with three C_2 rotation axes along with two vertical mirror planes σ_v and one horizontal mirror plane σ_h. The last group of particles that we discuss here are the bent-core particles and kites with symmetry group C_{2v}. This symmetry group consists of one two-fold rotation axis C_2 and two mirror planes σ_d and σ_h.

In liquid crystal physics, you will notice a trend in naming particle shapes after fruits. For example, pear-shaped particles are a special case of polar rods. Another important example are banana-shaped particles which are similar to bent-core particles.

CHAPTER 2

Liquid crystals of banana-shaped particles

2.1 Phases of a liquid crystal of banana-shaped particles

The focus of this thesis is on liquid crystals of bent-core or banana-shaped colloidal particles with C_{2v} symmetry, also called bent-core mesogens [14]. As shown in Fig. 2.1(a), the particle orientation can be described by three axes: the polar axis $\boldsymbol{m}_1$, the long axis $\boldsymbol{m}_2$ (the notation $\boldsymbol{u}_i$ is also used, where i labels the particles), and the perpendicular axis $\boldsymbol{m}_3$. In the uniaxial nematic phase (see Fig. 2.1(b)), the long axes of the particles are aligned along the nematic director $\boldsymbol{n}$, while the particles are randomly oriented in the plane perpendicular to $\boldsymbol{n}$. However, the banana-like shape of the particles can stabilize other nematic phases, in which the particles are also transversely aligned in the plane perpendicular to $\boldsymbol{n}$, due to the polar order (see Fig. 2.1(c)).

In 1969, Meyer identified the bend flexoelectric effect as the mechanism responsible for the coupling between the nematic director and the polar order [16]. He argued that this effect either occurs because of electrostatic polarization of the liquid crystal, or due to the polarized particle shape in absence of an electric field. In Fig. 2.3, the bend flexoelectric effect for a liquid crystal of banana-shaped particles is illustrated. As a result, Oseen-Frank-like bend deformations can be induced in the nematic director. Since these bend deformations cannot be extended in three

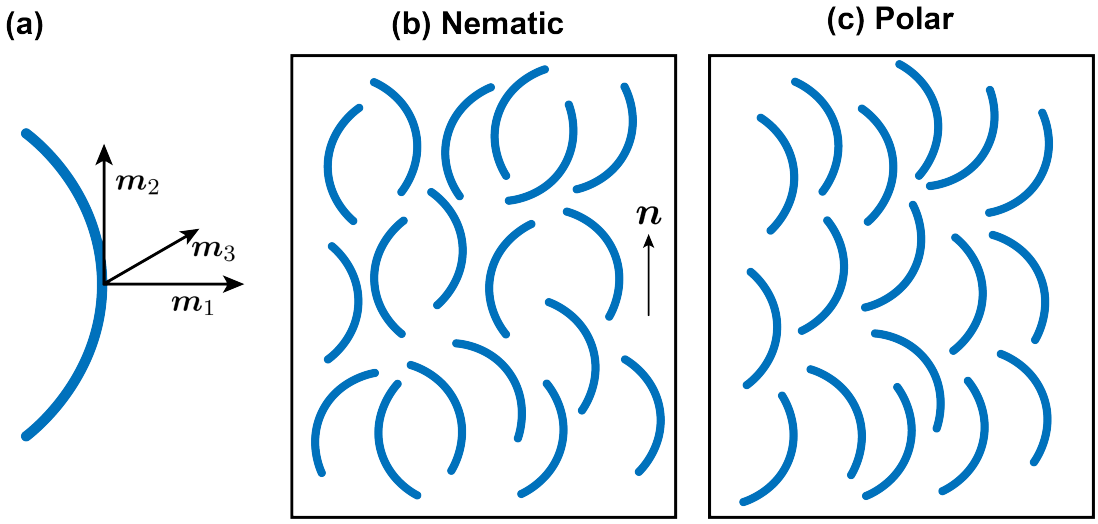

Figure 2.1: (a) Schematic representation of the orientation of a particle expressed in three vectors $\boldsymbol{m}_1, \boldsymbol{m}_2$ and $\boldsymbol{m}_3$, and two possible ways in which banana-shaped particles can align in a liquid crystal: (b) along the long axis forming a uniaxial nematic phase with up-down symmetry and (c) along both the long axis and the polar axis forming a polar phase.

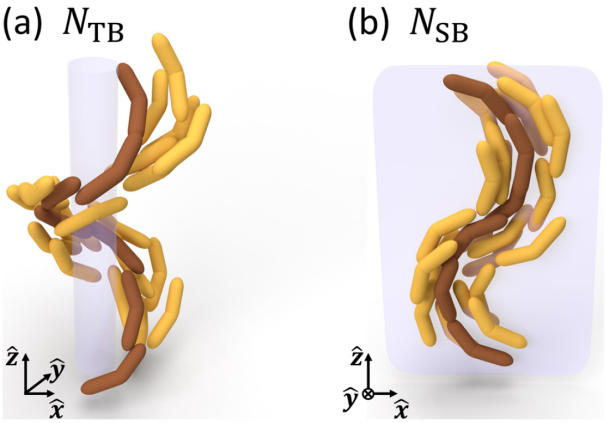

Figure 2.2: (a) The twist-bend nematic (N_{TB}) phase and (b) the splay-bend nematic (N_{SB}) phase. Figure from Ref. [15].

dimensions, the induced geometrical frustration is resolved by the emergence of either a twist or a splay distortion. The two resulting phases are the twist-bend nematic phase (N_{TB}) and the splay-bend nematic phase (N_{SB}), shown in Fig. 2.2. The N_{TB} phase is a chiral nematic phase characterized by an oblique heliconical arrangement of the nematic director. The N_{SB} on the other hand is characterized by alternating domains of splay and bend deformations.

2.2 Computational and experimental findings

2.2.1 Twist-bend and splay-bend phases

Since the postulation of the N_{TB} and the N_{SB} phase, the N_{TB} phase has been observed in experiments [18], unlike the N_{SB} phase. This has raised doubts on the existence of the N_{SB} phase. However, in 2019, Chiappini *et al.* showed with computer simulations that by destabilizing the smectic phase, a stable N_{SB} could be observed (among other stable phases) [5]. They were able to "lift the smectic blanket" by introducing either a polydisperse distribution of particle lengths or curvature in the particle shape. A sharp kink in the particle shape favors the formation of smectic clusters and therefore drives the phase transition towards a smectic phase. Introducing particle curvature not only destabilizes the smectic phase but also promotes bend deformations, resulting in a preference for $N_{TB} - N_{SB}$ transition over the $N_{TB} - \mathrm{Sm}$ transition.

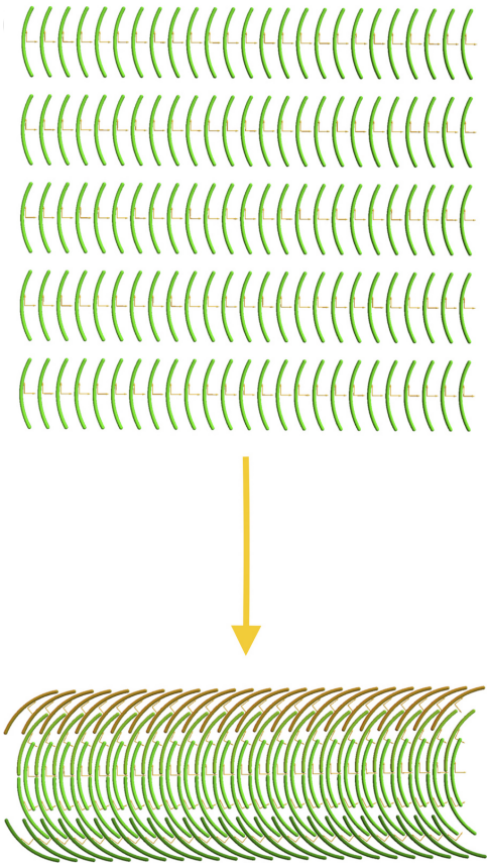

Figure 2.3: A sketch of the bend flexoelectric effect in a system of banana-shaped particles that shows how the polar order leads to bend deformations of the nematic director field. Figure adapted from Ref. [17].

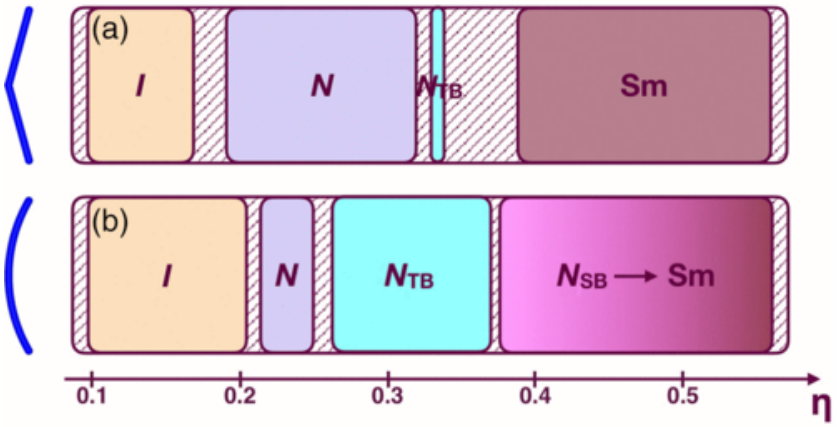

Figure 2.4: Phase diagram of (a) hard bent spherocylinders and (b) hard curved spherocylinders as a function of packing fraction η for a length-to-diameter ratio $L/D = 10$ and a opening angle of $\Psi = 150°$C. Figure from Ref. [5].

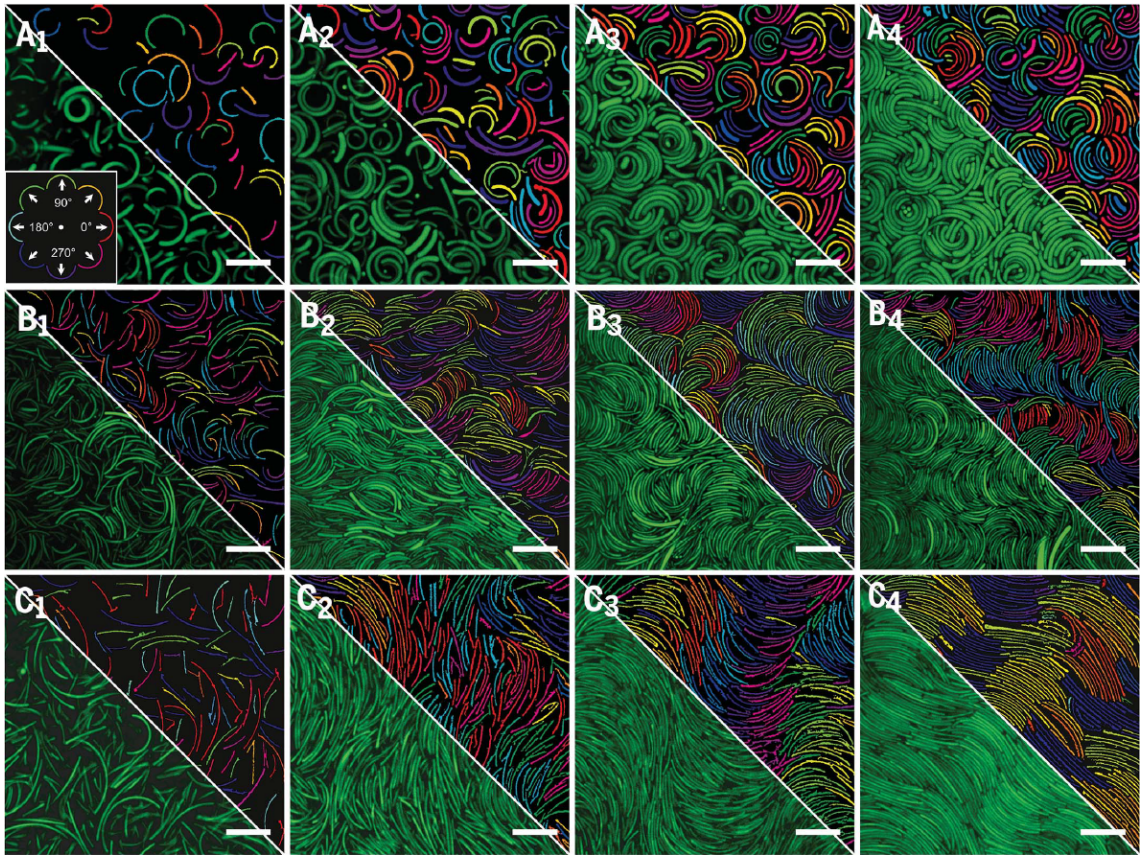

Figure 2.5: Phase behaviour of banana-shaped colloidal particles with $(A_1 - A_4)$ high curvature, $(B_1 - B_4)$ medium curvature, and $(C_1 - C_4)$ low curvature for increasing packing fractions from left to right. Figure from Ref. [6].

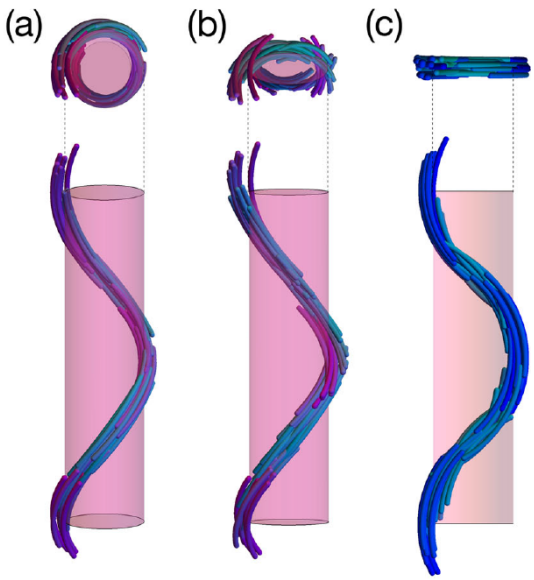

Figure 2.6: Side and top views of the (a) twist-bend, (b) twist-splay-bend, and (c) splay-bend phases of banana-shaped particles. The long axes of two particles with the same color are aligned. Figure from Ref. [19].

Fig. 2.4 shows the effect of introducing curvature on the phase diagram as a function of packing fraction η for banana-shaped particles with a length-to-diameter ratio $L/D = 10$ and a opening angle of $\Psi = 150$°C. For hard bent spherocylinders, as shown in Fig. 2.4(a), the phase sequence is $I - N - N_{\mathrm{TB}} - \mathrm{Sm}$ where a small regime of the twist-bend phase is followed by a first-order phase transition to a smectic phase. However, for hard curved spherocylinders, the first-order $N_{\mathrm{TB}} - \mathrm{Sm}$ phase transition is replaced by a weak first-order phase transition from N_{TB} to N_{SB} followed by a second-order phase transition to a smectic phase. This shows that the N_{TB} and N_{SB} phases are metastable compared to the smectic phase for hard bent spherocylinders. By destabilizing the smectic phase, these more exotic phases can be observed.

A year later, Fernández-Rico *et al.* found the phase behaviour of banana-shaped colloidal particles as a function of the particle curvature and the packing fraction, shown in Fig. 2.5, using an experimental setup. They showed that highly-curved particles only show isotropic behaviour as a function of packing fraction (see Fig. 2.5A), while less curved bananas show isotropic, biaxial and smectic phase behaviour as well as a splay-bend phase (see Fig. 2.5C_3). This confirms the existence of a splay-bend phase which becomes stable upon destabilizing the smectic phase.

2.2.2 The intermediate twist-splay-bend phase

In 2021, Chiappini *et al.* found that the twist-bend phase (Fig. 2.6(a)) transitions to a splay-bend phase (Fig. 2.6(c)) via an intermediate twist-splay-bend phase N_{TSB} (Fig. 2.6(b)) [19]. This intermediate phase displays modulations of all three deformations (twist, splay and bend), which means that the bend deformations need not necessarily only be accompanied by a twist or a splay deformation, but also by both deformations simultaneously. The $N_{\mathrm{TB}} - N_{\mathrm{TSB}} - N_{\mathrm{SB}}$ phase transition happens continuously, where the twist deformations are gradually replaced by splay deformations.

As can be seen from the phase diagram obtained with Monte Carlo simulations in Fig. 2.7, a liquid crystal of curved spherocylinders undergoes several phase transitions in a specific order as a function of the packing fraction. For small particle curvatures, the phase sequence is $I - N - N_{\mathrm{TB}} - N_{\mathrm{TSB}} - N_{\mathrm{SB}}$. However, the stability range of the nematic phases decreases for

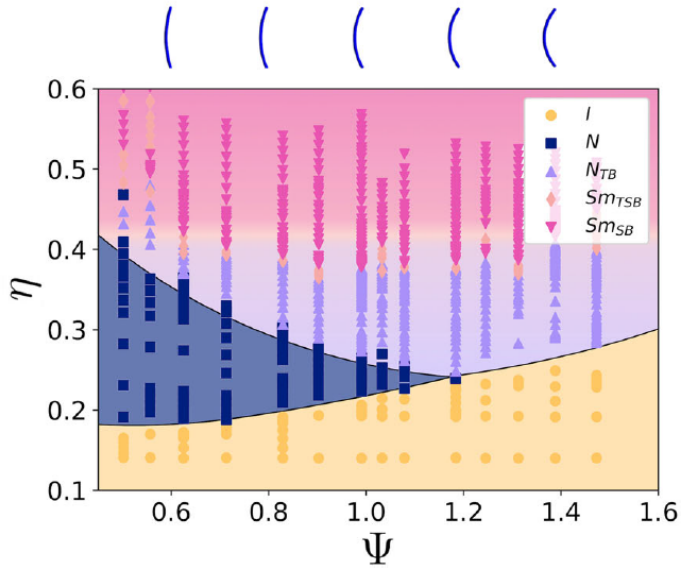

Figure 2.7: A phase diagram of curved spherocylinders obtained from simulations as a function of the packing fraction η and the particle curvature Ψ. Figure from Ref. [19].

higher particle curvatures, resulting in a different phase sequence. Notice that the twist-splay-bend and the splay-bend phase are denoted as smectic phases $\mathrm{Sm_{TSB}}$ and $\mathrm{Sm_{TSB}}$ in Fig. 2.7. Because splay deformations are coupled to density modulations, these two phases are actually more characteristic of a smectic phase rather than a nematic phase. This will be discussed further in Section 3.4.3.

CHAPTER 3

Landau-de Gennes theory

3.1 Landau theory

In 1937, Landau introduced a general theory for continuous or second-order phase transitions [20], which can also be adapted to describe first-order phase transitions. In this theory, the free energy should be analytic and obey the symmetries of the Hamiltonian. One can then write down the free energy as an expansion in terms of an order parameter, which is a measure of the degree of ordering in a system, and is often taken to be zero in a disordered phase and nonzero in an ordered phase. This means that a phase transition can be characterized by an order parameter. Since Landau theory describes the universal behaviour of a system, it is used to study many different phase transitions.

Consider the Landau expansion of the free energy at temperature T, given by

$$f(T,m) = f_0(T) + a(T)m + b(T)m^2 + c(T)m^3 + d(T)m^4 + \dots, \tag{3.1}$$

where $a, b, c, d, \dots$ are expansion coefficients and m is the scalar order parameter of an anisotropic magnetic model with broken up-down symmetry. To adapt this expansion for a given system, the coefficients are chosen such that they respect the symmetry of the disordered phase. We know that the disorder phase occurs at $m = 0$, resulting in the free energy having a minimum at $m = 0$ for temperatures T above the critical temperature T_c. This fixes the first coefficient a at zero since the linear term must be zero for f to have a minimum at $m = 0$. Secondly, the free energy must have a local minimum at $m = 0$ for the disordered phase to be stable for $T > T_c$. That means the second derivative of f must be positive at $m = 0$, hence $b > 0$ for $T > T_c$. To ensure stability of the disordered phase, we also need the free energy to diverge for $m \to \infty$. Therefore, $d > 0$ for all T. Now, one can distinguish two cases: either $c = 0$ or $c \neq 0$. A free energy without the third-order term indicates the existence of a continuous or second-order phase transition, while the presence of a third-order term yields a discontinuous or first-order phase transition. To summarize, with a Landau expansion of the free energy, one can determine the regions of stability for each phase and predict the type of phase transition (first-order/discontinuous or second-order/continuous) that will occur.

3.2 The order parameter

One of the phase transitions that can be described with Landau theory is the isotropic to nematic ($I-N$) phase transition of a liquid crystal. Because this is a symmetry-breaking phase transition, the two phases can be described with an order parameter. In an $I-N$ phase transition, the order parameter is zero in the ordered or isotropic phase, and nonzero in the disordered or nematic phase. In this section, we will derive the form of this order parameter.

Consider a nematic phase of rod-like and rigid particles. We can introduce a unit vector $\boldsymbol{u}_i$ along the long axis of the ith particle to describe its orientation. Since this system has up-down symmetry, the average of the unit vectors vanishes. This suggests that the $I-N$ phase transition cannot be described by a vector order parameter. It turns out that in order to describe the phase transition correctly, the order parameter should be a second-rank tensor $\boldsymbol{Q}$ with the following properties [21]:

1. $\boldsymbol{Q}$ is symmetric, i.e. $Q_{\alpha\beta} = Q_{\beta\alpha}$,
2. $\boldsymbol{Q}$ is traceless, i.e. $\operatorname{Tr} Q_{\alpha\beta} = 0$,
3. In the isotropic phase, $Q_{\alpha\beta} = 0$.

Note that the first two properties reduce the number of independent components from 9 to 5.

The most general form of a second-rank tensor with these properties is

$$Q_{\alpha\beta}(\boldsymbol{r}) = \frac{3}{2N} \sum_{i=1}^{N} \left(u_\alpha^{(i)} u_\beta^{(i)} - \frac{1}{3}\delta_{\alpha\beta} \right), \tag{3.2}$$

where the sum is over N particles in a small volume at position $\boldsymbol{r}$ and $\alpha, \beta = x, y, z$.

In general, $\boldsymbol{Q}$ has three eigenvalues and three corresponding eigenvectors. There exists a basis in which the tensor is diagonal, with diagonal elements $-\frac{1}{2}S + \Delta, -\frac{1}{2}S - \Delta, S$. Here, S is the scalar nematic order parameter, which is a measure of the degree of alignment of the particles, while Δ is a measure of the biaxiality. The largest eigenvalue of $\boldsymbol{Q}$ is $\frac{2}{3}S$. The corresponding eigenvector is called the nematic director $\boldsymbol{n}(\boldsymbol{r})$. It represents the direction of preferred orientation of the particles near position $\boldsymbol{r}$. Because of the up-down symmetry of the particles, $\boldsymbol{n}(\boldsymbol{r})$ and $-\boldsymbol{n}(\boldsymbol{r})$ are equivalent.

For a uniaxial nematic phase where the particle distribution function has axial symmetry, $\Delta = 0$ and hence two of the eigenvalues are equal. This gives for the tensor order parameter

$$Q_{\alpha\beta}(\boldsymbol{r}) = \frac{3}{2}S \left(n_\alpha(\boldsymbol{r}) n_\beta(\boldsymbol{r}) - \frac{1}{3}\delta_{\alpha\beta} \right), \tag{3.3}$$

where n_α are the components of the nematic director $\boldsymbol{n}$. Note that in general $S = S(\boldsymbol{r})$, i.e. S could be spatially inhomogeneous. We can, without loss of generality, choose in the direction of the z-axis, i.e. $\mathbf{n} = (0, 0, 1)^T$, since these expressions are rotationally invariant. The tensor order parameter $\boldsymbol{Q}$ then becomes

$$\boldsymbol{Q} = \begin{pmatrix} -\frac{1}{2}S & 0 & 0 \\ 0 & -\frac{1}{2}S & 0 \\ 0 & 0 & S \end{pmatrix}. \tag{3.4}$$

3.3 Landau-de Gennes theory

Landau-de Gennes theory is a special case of Landau theory for nematic liquid crystals with a tensor order parameter as described in Section 3.2. Because the free energy is a scalar, it can only depend on invariant contractions of $\boldsymbol{Q}$, such as $Q_{\alpha\beta}Q_{\beta\alpha} = \operatorname{Tr}(\boldsymbol{Q}^2)$, where we use the Einstein convention to sum over repeated indices. The most general expansion of the free energy has the form

$$F = F_0 + A(T - T^*) \operatorname{Tr}(\boldsymbol{Q}^2) - B \operatorname{Tr}(\boldsymbol{Q}^3) + C \operatorname{Tr}(\boldsymbol{Q}^2)^2 + \mathcal{O}(\boldsymbol{Q}^5), \tag{3.5}$$

where A, B and C are phenomenological constants, T is the temperature and T^* is the temperature of the isotropic spinodal. Only the quadratic term changes sign as a function of temperature, which drives the phase transition. Actually, this form of the free energy only applies to thermotropic liquid crystals, since the associated phase transition occurs as a function of temperature. The lyotropic liquid crystals we are considering become ordered as a function of density. Therefore, the grand potential Ω should be used instead of the Helmholtz free energy F [22]. Consequently, the expansion parameters will depend on the chemical potential μ rather than the temperature. The density jump will be naturally be included through

$$\partial(\Omega/V)/\partial\mu|_{V,T} = -\rho, \tag{3.6}$$

where V is the volume of the system and ρ the average density.

Consider hard rods of length L and diameter D at a chemical potential μ. Assuming that the grand potential will only depend on $\boldsymbol{Q}$ and its gradient $\nabla\boldsymbol{Q}$, we find

$$\Delta\Omega[\boldsymbol{Q}] = \int_V d\boldsymbol{r}\left[\Delta\omega_b(\boldsymbol{Q}(\boldsymbol{r})) + \omega_e(\nabla\boldsymbol{Q}(\boldsymbol{r}))\right], \tag{3.7}$$

where ω_b is the excess bulk grand potential density with respect to the isotropic phase and ω_e corresponds to the elastic deformations and surface tension effects. Expanding the bulk grand potential density in terms of the lowest-order frame-invariant contractions of $\boldsymbol{Q}$, up to fourth order, gives

$$\begin{aligned}\beta B_2\Delta\omega_b(\boldsymbol{Q}(\boldsymbol{r}),\mu) &= \frac{2}{3}a\beta(\mu^*-\mu)\,Q_{\alpha\beta}Q_{\beta\alpha} - \frac{4}{3}b\,Q_{\alpha\beta}Q_{\beta\lambda}Q_{\lambda\alpha} + \frac{4}{9}d\,Q_{\alpha\beta}Q_{\beta\alpha}Q_{\lambda\rho}Q_{\rho\lambda}\\ &= \frac{2}{3}a\beta(\mu^*-\mu)\ \mathrm{Tr}\left(\boldsymbol{Q}^2\right) - \frac{4}{3}b\ \mathrm{Tr}\left(\boldsymbol{Q}^3\right) + \frac{4}{9}d\ \mathrm{Tr}\left(\boldsymbol{Q}^2\right)^2\end{aligned} \tag{3.8}$$

Here, double indices are summed over, and we will make use of Einstein notation in the remainder of this thesis. Furthermore, the second virial coefficient $B_2 = \pi L^2 D/4$ is used to make the Landau coefficients a, b, d dimensionless which are independent of μ for simplicity. Here, μ^* is the chemical potential where the quadratic term changes sign and hence defines the spinodal of the isotropic-to-nematic phase transition. Stability requires $a > 0$ and $d > 0$ as explained in Section 3.1 and $b > 0$ allows us to describe a first-order isotropic-to-nematic phase transition.

Similarly, expanding the grand potential term describing elastic deformations and surface tension effects up to square gradients of $\boldsymbol{Q}$ gives

$$\beta B_2\omega_e(\nabla\boldsymbol{Q}(\boldsymbol{r})) = \frac{2}{9}\Big[l_1(\partial_\alpha Q_{\beta\lambda})(\partial_\alpha Q_{\beta\lambda}) + l_2(\partial_\alpha Q_{\alpha\lambda})(\partial_\beta Q_{\beta\lambda}) - l_3 Q_{\alpha\beta}(\partial_\gamma Q_{\alpha\gamma})(\partial_\lambda Q_{\beta\lambda})\Big], \tag{3.9}$$

where the elastic constants l_1, l_2, l_3 are in units of L^2. There is another second-order term in $\nabla\Omega$, $(\partial_\alpha Q_{\beta\lambda})(\partial_\lambda Q_{\beta\alpha})$, but this term can be written as a linear combination of a surface term and the other two elastic terms in Eq. (3.9) [15]. The third term is necessary to break the degeneracy between the splay and bend elastic constants K_{11} and K_{33}, but this is only one of the possible couplings of $\boldsymbol{Q}$ and $\nabla\boldsymbol{Q}$ and other terms could have been used instead [15].

The grand potential term ω_e in Eq. (3.9) can be compared to the Oseen-Frank elastic energy in Eq. (1.1). We then find up to second order in S

$$K_{11} = K_{33} = 2S^2\frac{(l_1 + l_s)}{\beta B_2} \tag{3.10}$$

$$K_{22} = 2S^2\frac{l_1}{\beta B_2}, \tag{3.11}$$

where $l_s = \frac{1}{2}(l_2 + l_3)$. Any terms corresponding to the saddle-splay distortion are not taken into account for simplicity.

Landau-de Gennes theory is a phenomenological theory, which means that it is not based on the microscopic details of colloidal particles in a liquid crystal. It simply aims to describe the macroscopic phase transitions that can be observed. This means that either experimental data, computational data or information from a microscopic theory is needed to obtain values for the expansion parameters. For example, one can choose the values of the Landau coefficients a, b, d in such a way that the densities, chemical potentials and order parameter at isotropic-nematic coexistence correspond with those known from density functional theory. In the following sections, we will use results from Onsager theory [4]. Onsager theory will be more thoroughly discussed in Chapter 4.

3.3.1 Bulk properties

In the bulk phase we can assume a fully uniaxial nematic phase with $\boldsymbol{Q}$ as in Eq. (3.4). After a straightforward calculation one then determines $\mathrm{Tr}\,(\boldsymbol{Q}) = 0$, $\mathrm{Tr}\,(\boldsymbol{Q}^2) = \frac{3}{2}S^2$, and $\mathrm{Tr}\,(\boldsymbol{Q}^3) = \frac{3}{4}S^3$. Using this, we can express Eq. (3.8) in terms of the scalar order parameter S as

$$\beta B_2 \Delta\omega_b = a\beta(\mu^* - \mu)\, S^2 - b\, S^3 + d\, S^4. \tag{3.12}$$

Minimizing this with respect to S gives

$$\begin{aligned} S_I(\mu) &= 0; \\ S_N^{\pm}(\mu) &= \frac{3b}{8d}\left(1 \pm \sqrt{1 - \frac{32ad\beta(\mu^* - \mu)}{9b^2}}\right), \end{aligned} \tag{3.13}$$

where S_I corresponds to the order parameter in the isotropic phase and $S_N^{\pm}$ are the two solutions for the nematic phase. The stability of these solutions can be investigated by looking at the sign of $\partial^2\Delta\omega_b/\partial S^2$. Since $\partial^2\Delta\omega_b/\partial S^2|_{S=S_N^-} < 0$ for $\mu > \mu^*$, the solution $S_N^-(\mu)$ is a local maximum rather than a minimum. That means S_I and $S_N^+ \equiv S_N$ are the possible minimum solutions for the isotropic and nematic phase respectively.

Next, the chemical potentials at important points during the phase transition need to be determined. The chemical potential μ^* corresponding to the spinodal of the isotropic phase can be found from the condition $\partial^2\Delta\omega_b/\partial S^2|_{S=S_I} = 0$. Secondly, $\beta\mu^+ = \beta\mu^* - 9b/(32ad)$ corresponds to the spinodal of the nematic phase and is the chemical potential for which the condition $\partial^2\Delta\omega_b/\partial S^2|_{S=S_N^+} = 0$ holds. Lastly, the binodal corresponding to the $I - N$ transition is given by $\beta\mu_{IN} = \beta\mu^* - b^2/(4ad)$ which corresponds to the solution of $\Delta\omega_b(S_I) = \Delta\omega_b(S_N^+)$.

The solution $S_I(\mu) = 0$ corresponds to the isotropic phase which is stable for $\mu < \mu_{IN}$ since it is a global minimum. For $\mu_{IN} < \mu < \mu^*$, the solution is a local minimum which means that the isotropic phase is metastable. The isotropic phase becomes unstable for $\mu > \mu^*$ where the solution stops being a local minimum.

The nematic phase has two solutions $S_N^{\pm}(\mu)$ which only exist for $\mu > \mu^+$. The negative solution S_N^- is a local maximum and thus absolutely unstable for $\mu^+ < \mu < \mu^*$. From $\mu > \mu^*$, the negative solution of the nematic phase becomes unstable. The positive solution is always a minimum in the region where it exists. For $\mu^+ < \mu < \mu^*$ this minimum is local, so the nematic phase is metastable. From $\mu > \mu^*$, the positive solution nematic phase becomes a global minimum so the nematic phase becomes stable. The stability of all these branches is shown in Fig. 3.1, where we used the values obtained from fits to Onsager theory as explained below.

The chemical potential can be converted to the dimensionless density $c = B_2\rho$. Introduce the grand potential density of the isotropic phase ω_I, such that $\omega = \omega_I + \Delta\omega_b$. Rewriting Eq. (3.6) as the condition $\partial(B_2\omega)/\partial\mu = -c$, we find

$$c(\mu) = c_I(\mu) + aS^2, \tag{3.14}$$

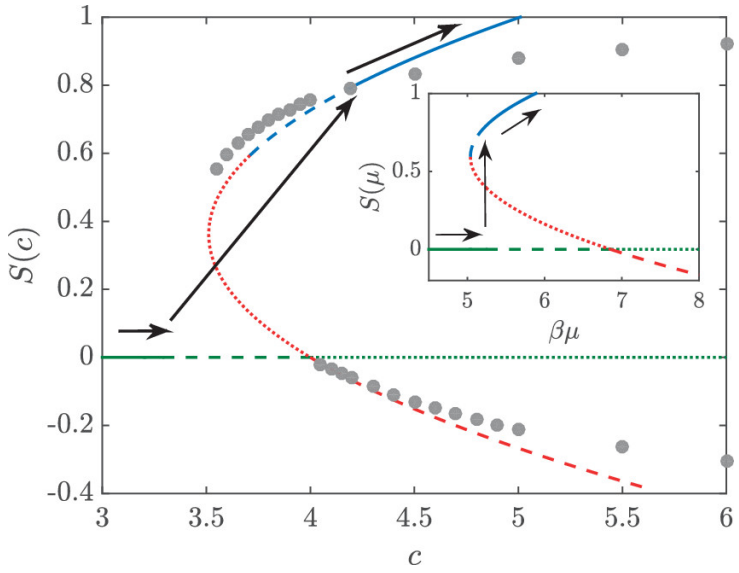

Figure 3.1: Bifurcation diagram of a Landau-de Gennes theory for hard rods in the density-order parameter (c, S) representation and the chemical potential-order parameter (μ, S) representation with the coefficients obtained from fits to Onsager theory. Full lines indicate the branch is globally stable, while dashed and dotted lines are used to indicate metastability and absolute instability respectively. The grey dots show the data points obtained from Onsager theory.

where c_I is defined as $-\partial(B_2\omega_I)/\partial\mu$ and can be obtained within Onsager theory by using an isotropic distribution function, such that $\beta\mu(c_I) = \log(c_I/4\pi)+2c_I$ [23]. Inverting this expression gives $c_I(\mu)$. At coexistence, we then have

$$\begin{cases} c(\mu_{IN}) = c_I(\mu_{IN}) + aS_{IN}^2 \\ \beta\mu_{IN} = \beta\mu^* - b^2/(4ad) \\ S_{IN} = b/(2d) \end{cases} \tag{3.15}$$

To obtain the Landau coefficients a, b and d, we fit them to the results from Onsager theory at isotropic-nematic coexistence. For a system of hard rods in the limit of $L/D \to \infty$, it is known within Onsager theory that $c_I(\mu_{IN}) = 3.290$, $c(\mu_{IN}) = 4.191$, $\beta\mu^* = 6.855$, $\beta\mu_{IN} = 5.241$, and $S_{IN} = 0.7922$ [23]. Using these values, we then find $a = 1.436$, $b = 5.851$, and $d = 3.693$. We further determine that $\beta\mu^+ = 5.039$. The bifurcation diagram in the (c, S) and (μ, S) representation is shown in Fig. 3.1, where the stable, metastable and unstable regions are indicated with full, dashed and dotted lines. The arrows indicate the isotropic to nematic phase transition and clearly show the density jump in the (c, S) representation. The results from our Landau-de Gennes theory match well with the data obtained from Onsager theory shown in grey dots, where the perfect agreement at coexistence is by construction and deteriorates at higher densities.

3.3.2 Isotropic-nematic interface

As shown in the previous section, by solving the Euler-Lagrange equation $\partial\Delta\omega_b[S]/\partial S = 0$, one can determine the value of the order parameter, the nature of the isotropic-to-nematic phase transition, and the stability of the different phases in the bulk. Now, consider an inhomogeneous system with an isotropic phase at $z \to \infty$ and a nematic phase at $z \to -\infty$ with bulk order parameter S_b. We assume homogeneity in the plane perpendicular to the z-axis. A planar interface will arise between these two phases with an order parameter profile $S(z)$ and a density profile $c(z)$. Let α be the angle between the nematic director and the normal of the interface.

For $\alpha = 0$, the rods are aligned perpendicular to the interface, while for $\alpha = \pi/2$ the rods are aligned parallel to the interface. The surface tensions $\gamma_\perp$ and $\gamma_\parallel$, corresponding to perpendicular and parallel anchoring respectively, are known within Onsager theory [24]. These can be used to fit two of the three elastic constants l_1 and $l_s = (l_2 + l_3)/2$ in Eq. (3.9).

The grand potential per unit area of the interface A is given by

$$\frac{\Delta\Omega[S]}{A} = \int dz \left[\Delta\omega_b\left(S(z);\mu\right) + \frac{m(\alpha)}{2\beta B_2}\left(S'(z)\right)^2\right], \tag{3.16}$$

where $m(\alpha)$ is the stiffness constant given by [22]

$$m(\alpha) = (2/3)\left[l_s\cos^2(\alpha) + l_1 + l_s/3\right]. \tag{3.17}$$

Upon rewriting the Euler-Lagrange equation $\delta\Delta\Omega[S]/\delta S = 0$, we find the minimisation condition

$$\begin{cases} m(\alpha)S''(z) = \dfrac{\partial\left[\beta B_2\Delta\omega_b\left(S(z)\right)\right]}{\partial S(z)} \\ \lim\limits_{z\to\infty} S(z) = 0, \quad \lim\limits_{z\to-\infty} S(z) = S_b \end{cases} \tag{3.18}$$

We can now consider this equation at coexistence where $\mu = \mu_{IN}$ and $S_b = S_{IN}$. Multiplying it with $S'(z)$ gives

$$\begin{aligned} m(\alpha)S''(z)S'(z) &= \frac{\partial\left[\beta B_2\Delta\omega_b\left(S(z)\right)\right]}{\partial S(z)}\frac{\partial S(z)}{\partial z} \implies \\ \frac{m(\alpha)}{2}\frac{\partial\left(S'(z)\right)^2}{\partial z} &= \frac{\partial\left[\beta B_2\Delta\omega_b\left(S(z)\right)\right]}{\partial z} \end{aligned} \tag{3.19}$$

Integrating over z gives

$$\beta B_2\Delta\omega_b = \frac{m(\alpha)}{2}\left(S'(z)\right)^2, \tag{3.20}$$

where the integration constant vanishes because $S'(z) \to 0$ for $z \to \pm\infty$. We can write the left-hand side of Eq. (3.20) in terms of S and S_{IN} by substituting μ_{IN} and S_{IN} from Eq. (3.15) into Eq. (3.12), which gives

$$\begin{aligned} \beta B_2\Delta\omega_b &= \frac{b^2}{4d}S^2 - b\,S^3 + d\,S^4 \\ &= d\,S_{IN}^2\,S^2 - 2d\,S_{IN}\,S^3 + d\,S^4 \\ &= d\,S^2\left(S - S_{IN}\right)^2 \end{aligned} \tag{3.21}$$

Combining Eq. (3.20) and Eq. (3.21) and taking the square root yields

$$\sqrt{\frac{m(\alpha)}{2}}S'(z) = \sqrt{d}\,S(z)\left(S(z) - S_{IN}\right), \tag{3.22}$$

where we take the positive root to ensure consistency with the boundary conditions. Rewriting gives

$$\begin{aligned} dz &= \sqrt{\frac{m(\alpha)}{2d}}\frac{dS}{S(S - S_{IN})} \\ &= \sqrt{\frac{m(\alpha)}{2d}}\cdot\frac{-1}{S_{IN}}\left(\frac{dS}{S} - \frac{dS}{S_{IN} - S}\right) \\ &= -\sqrt{\frac{m(\alpha)}{2d}}\frac{2d}{b}d\log\left(\frac{S}{S_{IN} - S}\right). \end{aligned} \tag{3.23}$$

Upon integrating, we then find

$$z = -\xi \log\left(\frac{S}{S_{IN} - S}\right), \tag{3.24}$$

where $\xi = \sqrt{2m(\alpha)d}/b$ is the correlation length. Inverting this equation yields the profile for the order parameter $S(z)$ and, using Eq. (3.14), the dimensionless density $c(z)$

$$S(z) = \frac{S_{IN}}{2}\left[1 - \tanh\left(\frac{z}{2\xi}\right)\right] \tag{3.25}$$

$$c(z) = c_I + \frac{aS_{IN}^2}{4}\left[1 - \tanh\left(\frac{z}{2\xi}\right)\right]^2. \tag{3.26}$$

At coexistence, $\Delta\omega_b(S_{IN}, \mu_{IN}) = 0$ by definition, so only the isotropic part of the grand potential ω_I contributes to the bulk pressure. Therefore, the surface tension $\gamma(\alpha)$ is equal to the grand potential $\Delta\Omega/A$ evaluated at coexistence

$$\begin{aligned}
\beta B_2 \gamma(\alpha) &= m(\alpha) \int_{-\infty}^{\infty} dz \, \left(S'(z)\right)^2 \\
&= m(\alpha) \int_{S_{IN}}^{0} dS(z) \, S'(z) \\
&= \sqrt{2m(\alpha)d} \int_0^{S_{IN}} dS \, (S^2 - SS_{IN}) \\
&= \sqrt{\frac{m(\alpha)d}{18}} S_{IN}^3,
\end{aligned} \tag{3.27}$$

where we used Eq. (3.22) going from the second to the third line. We can obtain $m(\alpha)$ by inverting Eq. (3.27), which yields

$$m(\alpha) = \frac{9}{8d}\left(\frac{\pi\beta\gamma(\alpha)LD}{S_{IN}}\right)^2 L^2 \tag{3.28}$$

Using the surface tensions known from Onsager theory, $\beta\gamma_{\parallel}LD = 0.156$ for $\alpha = \pi/2$ and $\beta\gamma_{\perp}LD = 0.265$ for $\alpha = 0$, we find $m_{\parallel} = 0.296L^2$ and $m_{\perp} = 0.854L^2$ [22]. Combining these numerical values with Eq. (3.17), we find for the elastic constants $l_1 = 0.165L^2$ and $l_s = 0.837L^2$. With the resulting Landau-de Gennes theory more complex systems can be studied, such as hedgehog defects, confined hard rods and nematic droplets [22].

3.4 An extended Landau-de Gennes theory

The Landau-de Gennes theory as described in Section 3.3 can be extended to describe liquid crystals of banana-shaped colloidal particles and its twist-bend and splay-bend phases [15]. Because of the bend flexoelectric effect, an additional order parameter $\boldsymbol{P}(\boldsymbol{r})$ is needed to describe the polar order. In the isotropic phase $\boldsymbol{Q} = 0 = \boldsymbol{P}$, in the uniaxial nematic phase $\boldsymbol{Q} \neq 0$ and $\boldsymbol{P} = 0$, and in the spatially modulated phases $\boldsymbol{Q} \neq 0 \neq \boldsymbol{P}$. The Landau-de Gennes grand potential is given by

$$\Delta\Omega[\boldsymbol{Q}, \boldsymbol{P}] = \int_V d\boldsymbol{r} \, \Big[\Delta\omega_b + \omega_e + \omega_P\Big], \tag{3.29}$$

where $\Delta\omega_b$ is the excess bulk grand potential density as in Eq. (3.8), and ω_e describes the elastic deformations and surface tension effects as in Eq. (3.9). The last term of Eq. (3.29) contains

the lowest-order contributions of the coupling between $\boldsymbol{Q}$ and $\boldsymbol{P}$ and its derivatives

$$\begin{aligned}\beta B_2\omega_p(\boldsymbol{Q},\boldsymbol{P},\nabla\boldsymbol{Q},\nabla\boldsymbol{P}) = e_2P_\alpha\Big(\delta_{\alpha\beta}+\frac{2}{S_0}Q_{\alpha\beta}\Big)P_\beta + e_4P_\alpha P_\alpha P_\beta P_\beta - \lambda P_\alpha(\partial_\beta Q_{\alpha\beta}) \\ + \kappa(\partial_\alpha P_\beta)(\partial_\alpha P_\beta) + e_6P_\alpha P_\alpha P_\alpha P_\beta P_\beta P_\beta,\end{aligned} \tag{3.30}$$

with coefficients $e_2, e_4, e_6, \kappa, \lambda, S_0$. This equation contains terms up to sixth order in $\boldsymbol{P}$ to allow for both first-order and second-order phase transitions to the spatially modulated phases. Stability requires $e_6 > 0$, but e_4 can be both positive or negative.

In the remainder of this section, we will use a system of hard rods with length-to-diameter ratio $L/D \to \infty$ as our reference system. That means that as in Section 3.3.2, the Landau coefficients and two of the three elastic constants can be chosen such that the results match with those known from Onsager theory. The nematic to twist-bend nematic ($N - N_{\mathrm{TB}}$) and the nematic to splay-bend nematic ($N - N_{\mathrm{SB}}$) phase transitions can then be studied as a function of the third elastic constant l_3. By solving the Euler-Lagrange equations $\partial\Delta\Omega/\partial S = 0$ and $\partial\Delta\Omega/\partial P = 0$, one can study the $N - N_{\mathrm{TB}}$ and $N - N_{\mathrm{SB}}$ phase transitions, and determine the stability and nature of the spatially modulated phases.

3.4.1 Second-order phase transitions

Let us now consider the simplest case where $e_6 = 0$ and $e_4 > 0$ to ensure stability. This will restrict all the possible phase transitions to second-order phase transitions. We can use the extended Landau-de Gennes theory to describe the phase behaviour of a lyotropic liquid crystal of banana-shaped particles, more specifically the nematic, nematic twist-bend and nematic splay-bend phases and phase transitions. To describe an N_{TB} phase, we first need a nematic director $\boldsymbol{n}_{\mathrm{TB}}(z)$ which precesses around the z-axis with an angle θ and a pitch $p = 2\pi/q$ (see Fig. 3.2), and secondly a polarization vector $\boldsymbol{P}_{\mathrm{TB}}(z)$ such that it is perpendicular to the nematic director,

$$\begin{aligned}\boldsymbol{n}_{\mathrm{TB}}(z) &= (\sin\theta\cos(qz), \sin\theta\sin(qz), \cos\theta)\,, \\ \boldsymbol{P}_{\mathrm{TB}}(z) &= P(z)\,(\sin(qz), -\cos(qz), 0)\,.\end{aligned} \tag{3.31}$$

Similarly, the nematic director and the polarization vector for the N_{SB} can be constructed

$$\begin{aligned}\boldsymbol{n}_{\mathrm{SB}}(z) &= (\sin\phi(z), 0, \cos\phi(z))\,, \\ \boldsymbol{P}_{\mathrm{SB}}(z) &= P(z)\psi(z)\,(-\cos\phi(z), 0, -\sin\phi(z), 0)\,,\end{aligned} \tag{3.32}$$

with $\psi(z) = \cos(qz)$ and $\phi(z) = \theta\sin(qz)$.

There exists a complete mapping between the Oseen-Frank theory of Dozov [25] and Selinger [26–28] and the extended Landau-de Gennes theory as introduced in Section 3.4 with $l_3 = 0$, i.e. a degenerate bend and splay elastic constant ($K_{11} = K_{33}$). The Oseen-Frank theory predicts the existence of a phase transition from the nematic phase to either an N_{TB} or an N_{SB} phase. Using the results from Ref. [15], the grand potential densities of the twist-bend and splay-bend phase are given by

$$\frac{\Delta\Omega_{\mathrm{TB}}}{V} = -\frac{16e_2^3S^2\,(2l_1+l_2)^4\,(S-S_c)^3}{729S_0^3\kappa\lambda^4l_1}, \tag{3.33}$$

$$\frac{\Delta\Omega_{\mathrm{SB}}}{V} = -\frac{64e_2^3S^2\,(2l_1+l_2)^3\,(S-S_c)^3}{729S_0^3\kappa\lambda^4}, \tag{3.34}$$

where the approximation is made that P is small. The $\Delta\Omega_{\mathrm{SB}}$ varies periodically as a function of z, so here it is averaged over one full period $2\pi/q$ as

$$\frac{\Delta\Omega_{\mathrm{SB}}}{V} = \frac{q}{2\pi}\int_0^{2\pi/q} dz\Delta\omega(z). \tag{3.35}$$

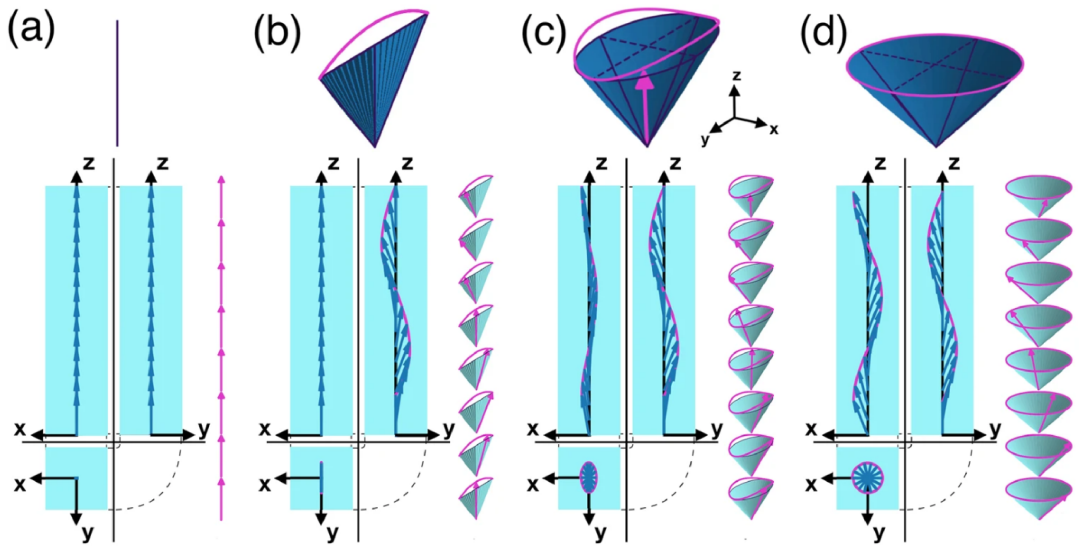

Figure 3.2: Precession cone (top) and orthogonal projection of the nematic director field (bottom) of a (a) uniaxial nematic phase, (b) splay-bend phase, (c) twist-splay-bend phase, and (d) twist-bend phase. Figure adapted from Ref. [19].

S_c is the critical scalar nematic order parameter at which both $\Delta\Omega_{\mathrm{TB}}$ and $\Delta\Omega_{\mathrm{SB}}$ vanish for small P, given by

$$S_c = \mathrm{S}_0 \left(1 - \frac{9\lambda^2}{8e_2\,(2l_1 + l_2)}\right). \tag{3.36}$$

Calculating the ratio of the two grand potential densities using $K_{11} = S^2(2l_1 + l_2)$ and $K_{22} = S^2(2l_1)$ from Eq. (3.10) gives

$$\frac{\Delta\Omega_{\mathrm{TB}}}{\Delta\Omega_{\mathrm{SB}}} = \frac{2l_1 + l_2}{4l_1} = \frac{K_1}{2K_2}. \tag{3.37}$$

Looking at the ratio in Eq. (3.37) and the minus signs in front of the grand potential densities in Eqs. (3.33) and (3.34), we see that at $S = S_c$, an $N - N_T B$ phase transition will occur for $K_{11} < 2K_{22}$ and an $N - N_S B$ phase transition for $K_{11} > 2K_{22}$. This agrees well with the results from Dozov [25] and Selinger [27, 28].

However, Oseen-Frank theory and the extended Landau-de Gennes theory with $l_3 = 0$ cannot describe phase transitions between spatially modulated nematic phases, while Fig. 2.4 does suggest the occurrence of an N_{TB} to N_{SB} phase transition. To be able to describe these phase transitions, the degeneracy between the splay and bend elastic constants must be lifted. Allowing l_3 to be non-zero ensures that the ratio K_{11}/K_{22} depends on the order parameter S. Following the derivation from Ref. [15], one finds

$$\frac{\Delta\Omega_{\mathrm{TB}}}{\Delta\Omega_{\mathrm{SB}}} = \frac{2l_1 + l_2}{4l_1} + \frac{l_3}{8l_1}S \tag{3.38}$$

$$= \frac{K_1}{2K_2} + \frac{3l_3}{8l_1}S, \tag{3.39}$$

where $K_{11} = S^2(2l_1 + l_2 - Sl_3)$ and $K_{22} = S^2(2l_1)$ as in Eq. (3.10).

The critical scalar order parameter also changes for l_3 and is given by

$$S_c = \frac{-4l_1 - 2l_2 + S_0 l_3}{2l_3} + \sqrt{\frac{-9S_0\lambda^2}{4e_2 l_3} + \frac{(4l_1 + 2l_2 + S_0 l_3)^2}{4l_3^2}}. \tag{3.40}$$

Depending on the values of l_1, l_2 and l_3, one can distinguish two different cases. Either a nematic to N_{TB} transition occurs at $S = S_c$ followed by an N_{TB} to N_{SB} phase transition at $S > S_c$, or at $S = S_c$ there is a phase transition from the nematic phase to the N_{SB} followed by an $N_{\mathrm{SB}} - N_{\mathrm{TB}}$ transition at $S > S_c$ [15]. For $-1.25L^2 < l_3 < -1.0L^2$, the $N - N_{\mathrm{TB}} - N_{\mathrm{SB}}$ transition from Ref. [5] is reproduced.

3.4.2 First-order $N - N_{\mathrm{TB}}$ phase transition

Now, consider the case where $e_6 \neq 0$ and the sign of e_4 can vary. This allows first-order phase transitions to occur as well, at least in principle. For $e_4 < 0$, we expect a first-order phase transition, while for $e_4 => 0$ a second-order phase transition will occur. Using the results from Ref. [15], where $l_3 = 0$ for simplicity, we find different regimes

$$\begin{cases} \text{(i) } e_4 < -1.5 & \text{strong first-order } I - N_{\mathrm{TB}} \text{ transition,} \\ \text{(ii) } e_4 = -1.5 & \text{triple point of } I - N - N_{\mathrm{TB}}, \\ \text{(iii) } -1.5 < e_4 < 0 & \text{weak first-order } I - N - N_{\mathrm{TB}} \text{ transition,} \\ \text{(iv) } e_4 > 0 & \text{second-order } N - N_{\mathrm{TB}} \text{ transition,} \end{cases} \tag{3.41}$$

with $e_2 = 1$, $\lambda = 0.08L^2$, $\kappa = 0.1L^2$, $e_6 = 10$, and $S_0 = 0.85$. Here, λ is chosen such that $e_4 = -1$ marks the point where the $I - N$ transition is followed by an $N - N_{\mathrm{TB}}$ transition. The authors of Ref. [15] were not able to find a set of coefficients for which the nematic splay-bend phase was more stable than the nematic twist-bend phase, consistent with simulation results [5]. However, by setting $l_3 \neq 0$, the first-order $N - N_{\mathrm{TB}}$ transition could be followed by a first-order $N_{\mathrm{TB}} - N_{\mathrm{SB}}$ phase transition [15].

3.4.3 Coupling of splay deformations and density modulations

In contrast with the N_{TB} phase, the N_{SB} phase has never been observed in a system of a thermotropic liquid crystal banana-shaped particles [29]. However, a variety of smectic phases have been observed, which caused the nature of the splay-bend phase as a nematic phase to be questioned. Using the extended Landau-de Gennes formalism as described in Section 3.4 with different elastic constants $l_1 = 0.1L^2$ and $l_2 = 0.0427L^2$, the authors of Ref. [29] showed that in a splay-bend phase, the scalar nematic order parameter $S = S(z)$ varies periodically along one spatial dimension. This indicates a one-dimensional density modulation which is distinctive of a smectic phase rather than a nematic phase. It would thus be more correct to denote the splay-bend phase with $\mathrm{Sm}_{\mathrm{SB}}$. That also means that the $N - N_{\mathrm{SB}}$ is strictly-speaking a $N - \mathrm{Sm}$ transition. Furthermore, the polar order parameter P_{SB} and the particle concentration also display periodic modulations along the z-axis. The latter can be understood when looking at the coupling between S and c in Eq. (3.15), and is characteristic of a smectic phase.

The difference in nature of the twist-bend and splay-bend phase lies in the coupling of density modulations to splay deformations of the nematic director field $\boldsymbol{n}_{\mathrm{SB}}$. As shown in Ref. [29], the splay deformations $\nabla \cdot \mathbf{n}_{\mathrm{SB}}(z)$ are coupled to the concentration gradient $\nabla c_{\mathrm{SB}}(z)$ as

$$\nabla \cdot \mathbf{n}_{\mathrm{SB}}(z) = \frac{H}{2} \frac{\nabla c_{\mathrm{SB}}(z)}{(c_{\mathrm{SB}}(z) - c_I)} \cdot \mathbf{n}_{\mathrm{SB}}(z), \tag{3.42}$$

where H is a spatial constant that varies with the chemical potential μ. This relation suggests that splay deformations cannot exist without a concentration gradient.

3.5 Shortcomings of Landau-de Gennes theory

3.5.1 The phenomenological nature of Landau-de Gennes theory

At the time of writing, the framework presented in this chapter has not been able to describe more complicated phase transitions such as the $N_{\mathrm{TB}} - \mathrm{Sm}_{\mathrm{SB}}$ transition. The intermediate twist-splay-bend phase and the phase sequence $I - N - N_{\mathrm{TB}} - N_{\mathrm{TSB}} - \mathrm{Sm}_{\mathrm{SB}}$ have also not been found with the current Landau-de Gennes theory.

One of the possible explanations comes from the fact that we have been using a system of hard rods with $L/D \to \infty$ as our reference system for a bent-core mesogen. As mentioned before, the Landau-de Gennes theory is a phenomenological theory, which means that it requires numerical input from microscopic theories, computer simulations or experiments. Up until now, we have used the results from Onsager theory [23, 24] as input parameters, and were able to produce correct results for the isotropic to nematic phase transition. However, the results from Onsager theory are not sufficient to describe the more involved phase transitions we are considering. This obstacle can be overcome by using simulation results as input parameters, and a simulated liquid crystal of banana-shaped particles as reference system.

One could argue that the power of Landau theory is also its drawback: it can be applied to many different systems with all sorts of different phase transitions. This ability to generalize means that any specific details of the system need to be put into the theory by hand. For example, the fact that the nematic director $\boldsymbol{n}$ and the polarization vector $\boldsymbol{P}$ are perpendicular is not automatically included in the theory, but is added manually in Eqs. (3.31) and (3.32).

3.5.2 Defining the right order parameters

Another possible reason for why the intermediate twist-splay-bend phase cannot yet be described by our extended Landau-de Gennes theory is that in order to describe more complicated phases and their transitions, different or additional order parameters might be necessary. As we have seen in Section 3.2, a second-order 3×3 tensor order parameter is needed to build a Landau-de Gennes theory of hard rods. However, constructing a Landau-de Gennes theory for systems beyond hard rods is not trivial and might require several higher-order tensor order parameters to describe the full system.

Consider a banana-shaped particle with axes $\boldsymbol{m}_1, \boldsymbol{m}_2$, and $\boldsymbol{m}_3$ as in Fig. 2.1. Usually $\boldsymbol{m}_2$ plays the role of the main axis, but here $\boldsymbol{m}_1$ is considered the main axis since it overlaps with the main symmetry axis of a particle with C_{2v} symmetry. According to Ref. [13], one needs five orientational order parameters to describe a liquid crystal of banana-shaped particles, given by

$$\begin{aligned} \boldsymbol{Q}^{[0]} &= \langle 1 \rangle, \\ \boldsymbol{Q}^{[1]} &= \langle \boldsymbol{m}_1 \rangle, \\ \boldsymbol{Q}^{[2]} &= \langle \boldsymbol{m}_1^2 - \frac{1}{3}\mathbb{I} \rangle, \\ \boldsymbol{M}_1^{[2]} &= \langle \boldsymbol{m}_2^2 - \boldsymbol{m}_3^2 \rangle, \\ \boldsymbol{M}_2^{[2]} &= \langle 2\boldsymbol{m}_2\boldsymbol{m}_3 \rangle, \end{aligned} \tag{3.43}$$

where the superscript denotes the order of the tensor and $< \cdots >$ represents an average over all the particles i. Here, we have used the notation

$$\boldsymbol{m}_1\boldsymbol{m}_2 = \frac{1}{2}(\boldsymbol{m}_1 \otimes \boldsymbol{m}_2 + \boldsymbol{m}_2 \otimes \boldsymbol{m}_1), \tag{3.44}$$

$$\boldsymbol{m}_1^2 = \boldsymbol{m}_1 \otimes \boldsymbol{m}_1. \tag{3.45}$$

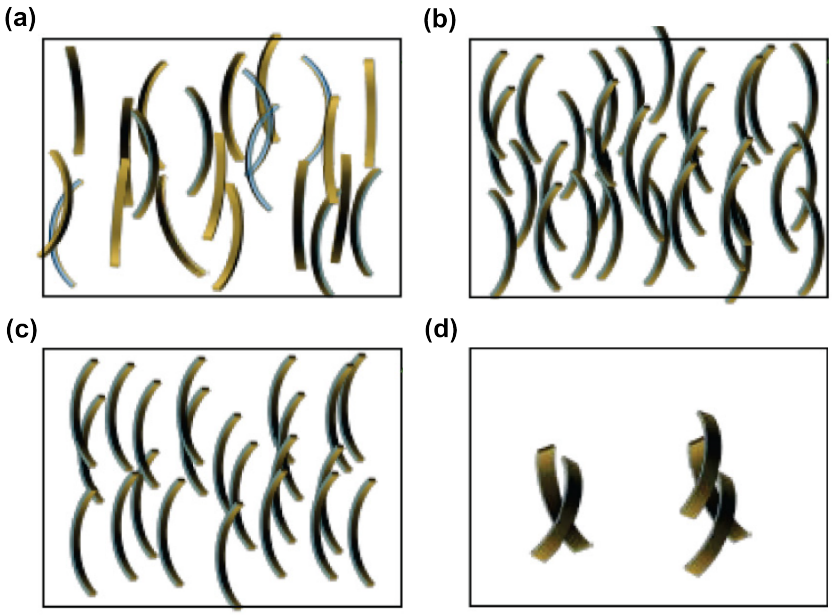

Figure 3.3: Different phases of a bent-core mesogen that are described by five order parameters: a (a) nematic phase, (b) biaxial phase, (c) polar phase, and (d) $\boldsymbol{M}_2^{[2]}$ phase. Figure adapted from Ref. [13].

The scalar $\boldsymbol{Q}^{[0]}$ characterizes the density variation which is needed to describe the smectic phases. Together with two second-order order parameters $\boldsymbol{Q}^{[2]}$ and $\boldsymbol{M}_1^{[2]}$, the nematic phase and the biaxial phase, where the particles also align in a plane, can be described (shown in Fig. 3.3(a) and (b) respectively). Adding the first-order tensor order parameter $\boldsymbol{Q}^{[1]}$ accounts for the polar phase, a phase in which the average of the $\boldsymbol{m}_1$ vectors is non-zero. The polar phase is shown in Fig. 3.3(c). Lastly, including the second-order tensor order parameter $\boldsymbol{M}_2^{[2]}$ gives rise to a new phase, shown in Fig. 3.3(d).

Returning to the order parameters $\boldsymbol{Q}$ and $\boldsymbol{P}$ introduced in Section 3.2 and Section 3.4, we can write them in terms of $\boldsymbol{m}_1, \boldsymbol{m}_2$, and $\boldsymbol{m}_3$ as

$$\begin{aligned} \boldsymbol{Q} &\sim \langle \boldsymbol{m}_2^2 - \frac{1}{3}\mathbb{I} \rangle, \\ \boldsymbol{P} &\sim \langle \boldsymbol{m}_1 \rangle. \end{aligned} \tag{3.46}$$

The order parameter $\boldsymbol{P}$ in our extended Landau-de Gennes theory is the same as the first-order tensor $\boldsymbol{Q}^{[1]}$, but $\boldsymbol{Q}$ does not appear in the list of five order parameters in Eq. (3.43). In addition, in order to be able to describe a biaxial phase, one would have to introduce a biaxial order parameter such as $\boldsymbol{M}_1^{[2]}$ or $\Delta = \frac{3}{2}\left\langle \boldsymbol{m}_3^2 - \frac{1}{3}\mathbb{I} \right\rangle$ in our extended Landau-de Gennes theory. Order parameters like $\boldsymbol{Q}^{[2]}$ and $\boldsymbol{M}_2^{[2]}$ are missing completely from our framework. Also note that the order parameters $\boldsymbol{Q}$ and $\boldsymbol{P}$ cannot be fully independent in the way that they are defined now since $\boldsymbol{m}_1$ and $\boldsymbol{m}_2$ are perpendicular.

This discussion clearly shows that defining the right set of order parameters to completely describe all phases of a liquid crystal is not trivial, especially when the internal symmetry group is smaller (i.e. the particle has a lower symmetry). This is also illustrated by the variety of approaches on this matter [13, 30]. It is therefore possible that we need additional order parameters to describe the more difficult phases such as the twist-bend, splay-bend and the intermediate twist-splay-bend phase.

3.5.3 Determining the full set of invariants

The next hurdle is determining the full set of invariants that can be constructed from the order parameter(s). This is not an easy or systematic process. In writing down the relevant invariants of $\boldsymbol{Q}$ and $\boldsymbol{P}$, choices of what to include and what to leave out had to be made. For example, in order to break the degeneracy between the splay and bend deformation, a term with $\boldsymbol{Q}$ and its derivative is included in Eq. (3.9). However, other couplings exist and could have been used instead. Similarly, in Eq. (3.30) only the lowest-order contributions have been included. It is possible that some of the higher-order contributions are relevant as well and are needed to describe more complicated phases. These choices are not trivial, which means it is difficult to prove that all the relevant terms have been included.

3.5.4 Choosing values for expansion coefficients

After defining the right order parameters and determining a full set of relevant invariants, one needs to choose the correct values for the expansion coefficients. There are some rules for simple systems, such that the second-order term must change sign at the phase transition, that higher-order even power terms are needed for stability, and that the coefficient in front of the highest-order term must be positive for stability reasons as well. However, for less symmetric particles the number of invariants and hence also the number of coefficients increases. This is were the lack of a systematic approach in choosing the right values for the expansion coefficients starts to cause problems.

The arguments above show that setting up a Landau-de Gennes theory is not easy and that a systematic approach is missing. Furthermore, because of the broad applicability of Landau theory, any information regarding the specifics of the system and the particles needs to be put into the theory by hand. An alternative to a phenomenological theory like Landau-de Gennes theory is a microscopic theory with density functional theory as a starting point. Building a microscopic theory for a liquid crystal of banana-shaped particles will be the focus of the remainder of this thesis.

CHAPTER 4

Density functional theory and bifurcation analysis

4.1 The density functional

Density functional theory (DFT) is a theoretical framework used to describe inhomogeneous and anisotropic phases. It is based on the proof that there exists a functional $\mathcal{W}[\rho]$ that is minimized by the equilibrium one-particle distribution ρ_{eq} [31]. If the pair potential of a particular type of particle is known, all of the thermodynamics can be derived from this functional by means of a variational principle. However, DFT does not tell us how to construct this functional. As a starting point, we know from the DFT framework that the functional in absence of an external potential can be written as

$$\mathcal{W}[\rho] = \mathcal{F}[\rho] - \mu \int d\boldsymbol{r} \int d\Omega\, \rho(\boldsymbol{r}, \Omega), \tag{4.1}$$

where $\mathcal{F}[\rho]$ is the intrinsic Helmholtz free energy functional, $\boldsymbol{r}$ the particle position, and Ω the orientation of the particle given by the three Euler angles α, β, γ.

The free energy functional consists of an ideal gas part, describing the free energy of a non-interacting system, and a non-ideal excess part, given by

$$\begin{aligned} \mathcal{F}[\rho] &= \mathcal{F}_{id}[\rho] + \mathcal{F}_{ex}[\rho] && (4.2)\\ &= \int d\boldsymbol{r} \int d\Omega\, \rho(\boldsymbol{r}, \Omega) \Big(\ln[\rho(\boldsymbol{r}, \Omega)\mathcal{V}] - 1 \Big) + \mathcal{F}_{ex}[\rho], && (4.3) \end{aligned}$$

with $\beta = 1/k_B T$ the inverse thermal energy, $\mathcal{V}$ the thermal volume a particle, and $d\Omega$ the integration measure such that

$$\int d\Omega = \int_0^{2\pi} d\alpha \int_0^{\pi} \sin\beta\, d\beta \int_0^{2\pi} d\gamma = 8\pi^2. \tag{4.4}$$

4.2 The Onsager approximation

As mentioned before, there is no straightforward way to construct the excess free energy functional. Here, we approximate $\mathcal{F}_{ex}[\rho]$ by a second virial expansion for the isotropic and homogeneous phase. Onsager showed that the higher-order virial terms can be neglected in systems of hard, rigid rods in the limit of infinite length-to-width ratio [4]. Although banana-shaped particles differ from these Onsager rods, we will use the Onsager approximation in the remainder of this thesis, as it is the one of the simplest possible approximations and catches the essential

physics of the isotropic-to-nematic transition. We can write the non-ideal part of the second virial free energy functional as

$$\beta\mathcal{F}_{ex}[\rho] = -\frac{1}{2}\int d\boldsymbol{r}\int d\boldsymbol{r}'\int d\Omega\int d\Omega'\, f(\boldsymbol{r},\Omega;\boldsymbol{r}',\Omega')\,\rho(\boldsymbol{r},\Omega)\,\rho(\boldsymbol{r}',\Omega'), \tag{4.5}$$

where f is the Mayer function given by

$$f(\boldsymbol{r},\Omega;\boldsymbol{r}',\Omega') = e^{-\beta U(\boldsymbol{r},\Omega;\boldsymbol{r}',\Omega')} - 1, \tag{4.6}$$

with $U(\boldsymbol{r},\Omega;\boldsymbol{r}',\Omega')$ the pair potential. We will assume global translational and rotational invariance, which means that the pair potential only depends on the relative position and orientation of the particles, i.e. $U(\boldsymbol{r},\Omega;\boldsymbol{r}',\Omega') = U(|\boldsymbol{r}-\boldsymbol{r}'|,\Omega,\Omega')$. Additionally, we will only consider hard particles, for which the pair potential is given by

$$\beta U(|\boldsymbol{r}-\boldsymbol{r}'|,\Omega,\Omega') = \begin{cases}\infty, & \text{if the particles overlap;}\\ 0, & \text{otherwise.}\end{cases} \tag{4.7}$$

The Mayer function then becomes

$$f(\boldsymbol{r},\Omega;\boldsymbol{r}',\Omega') = \begin{cases}-1, & \text{if the particles overlap;}\\ 0, & \text{otherwise.}\end{cases} \tag{4.8}$$

The full free energy functional in the Onsager approximation can now be written as

$$\begin{aligned}\beta\mathcal{F}[\rho] = &\int d\boldsymbol{r}\int d\Omega\,\rho(\boldsymbol{r},\Omega)\left(\ln[\rho(\boldsymbol{r},\Omega)\mathcal{V}]-1\right)\\ &-\frac{1}{2}\int d\boldsymbol{r}\int d\boldsymbol{r}'\int d\Omega\int d\Omega'\, f(\boldsymbol{r},\Omega;\boldsymbol{r}',\Omega')\rho(\boldsymbol{r},\Omega)\rho(\boldsymbol{r}',\Omega').\end{aligned} \tag{4.9}$$

Because the equilibrium distribution ρ_{eq} minimizes $\mathcal{W}[\rho]$, it must satisfy the stationarity condition

$$\left.\frac{\delta\mathcal{W}[\rho]}{\delta\rho(\boldsymbol{r},\Omega)}\right|_{\rho=\rho_{eq}} = \left.\frac{\delta\mathcal{F}[\rho]}{\delta\rho(\boldsymbol{r},\Omega)}\right|_{\rho=\rho_{eq}} - \mu = 0, \tag{4.10}$$

which ensures that only those fluctuations of $\rho(\boldsymbol{r},\Omega)$ are considered that conserve the normalization

$$\int d\boldsymbol{r}\int d\Omega\,\rho_{eq}(\boldsymbol{r},\Omega) = N. \tag{4.11}$$

Here, the chemical potential μ acts like a Lagrange multiplier that fixes the total number of particles.

4.3 Bifurcation analysis of spatially homogeneous phases

Density functional theory thus provides us with a thermodynamic equilibrium distribution of which the isotropic and homogeneous distribution is a solution. However, this solution is not necessarily stable, since it could also be a local maximum of $\mathcal{W}[\rho]$. In the regime(s) where this solution is no longer stable, an anisotropic and/or inhomogeneous distribution minimizes $\mathcal{W}[\rho]$ and could become stable. Determining this non-trivial solution can only be carried out numerically, but there exists an analytical tool which can give us information on the density at which the instability occurs and the characteristics of this non-trivial solution.

This tool is called bifurcation analysis, and it is a tool for studying the solutions of a self-consistency equation. Close to a phase transition, which is a symmetry breaking transition in

the case of liquid crystals, the Euler-Lagrange equation has two or more solutions. The isotropic phase is one solution which is stable up to a certain density. As the number density (or another parameter) is increased, the system branches out to a new solution, either immediately if it is a global minimum, or after the second solution becomes stable (instead of metastable). The density at which the second solution becomes stable with respect to the isotropic solution is known as the bifurcation density. This tool was introduced in the field of liquid crystals by Kayser and Ravaché in 1978 [32] and further developed by Mulder [33, 34]. This chapter is roughly based on their description.

For bifurcation analysis, a known stable solution such as the density in the isotropic phase is required, which is called the reference solution ρ_0. To find a solution close to the reference solution, we expand around the reference number density n_0 and get

$$n = n_0 + \epsilon n_1 + \epsilon^2 n_2 + \mathcal{O}(\epsilon^3), \tag{4.12}$$

where n_i are yet unknown coefficients and ϵ is a small arbitrary dimensionless parameter. Similarly, we can expand around the reference one-particle distribution function as

$$\rho = \rho_0 + \epsilon \left(\rho_1 + n_1 \rho_0'\right) + \epsilon^2 \left(\rho_2 + \frac{1}{2} n_1^2 \rho_0'' + n_2 \rho_0'\right) + \mathcal{O}(\epsilon^3). \tag{4.13}$$

Here, ρ_0' and ρ_0'' are the first and second derivative of ρ_0 with respect to n evaluated at $\epsilon = 0$. The flow along the reference solution, which is represented by these derivatives of ρ_0, is separated out. The deviations from the reference solution at every order in ϵ are then represented by the functions ρ_1 and ρ_2.

These expansions are then inserted into the free energy functional in the Onsager approximation from Eq. (4.9). Solving the stationarity condition Eq. (4.10) for the new free energy functional order by order in ϵ yields a solution that moves along the bifurcating solution branch. The bifurcation density n_0 can then be determined by the lowest-order self-consistent equation, also known as the (first) bifurcation equation, given by

$$\rho_1(\boldsymbol{r}, \Omega) = \rho_0(\boldsymbol{r}, \Omega) \int d\boldsymbol{r}' \int d\Omega' \, f(\boldsymbol{r}, \Omega; \boldsymbol{r}', \Omega') \rho(\boldsymbol{r}', \Omega'). \tag{4.14}$$

This is linear in ρ_1 and presumes ρ_0 known. In the case of multiple solutions around the bifurcation density, the true bifurcating solution is a linear combination of those solutions with the coefficients determined by higher order bifurcation equations.

Assume now that the one-particle distribution has no spatial dependence, such that $\rho(\boldsymbol{r}, \Omega) = n\psi(\Omega)$, with $n = N/V$ the number density, and $\psi(\Omega)$ the orientation distribution function with unit norm. Performing the integrals over the spatial degrees of freedom gives for the free energy functional

$$\frac{\beta \mathcal{F}[\psi]}{N} = \int d\Omega \, \psi(\Omega) \left(\ln \psi(\Omega) - 1\right) + \frac{1}{2} n \int d\Omega \int d\Omega' \, \mathcal{E}(\Omega, \Omega') \psi(\Omega) \psi(\Omega') + \ln(n\mathcal{V}). \tag{4.15}$$

Here, the Mayer function is replaced by the pair excluded volume $\mathcal{E}(\Omega, \Omega')$

$$\mathcal{E}(\Omega, \Omega') = -\int d\boldsymbol{r} \int d\boldsymbol{r}' f(\boldsymbol{r}, \Omega; \boldsymbol{r}', \Omega'), \tag{4.16}$$

which will turn out to play an important role in the bifurcation analysis. Working out the first bifurcation equation for a spatially homogeneous phase yields

$$\psi_1(\Omega) = -\frac{n_0}{8\pi^2} \int d\Omega' \, \mathcal{E}(\Omega, \Omega') \psi_1(\Omega'), \tag{4.17}$$

where the low density in the isotropic phase ψ_0 is replaced by $1/8\pi^2$.

Rewriting the first bifurcation equation as

$$|\psi_1\rangle = -\frac{n_0}{8\pi^2}\,\mathcal{E}\,|\psi_1\rangle \tag{4.18}$$

indicates that this is nothing but an eigenvalue problem. The bifurcation density is the minimum value of the density for which the eigenvalue of the excluded volume $\mathcal{E}$ is the most negative. The associated eigenvector describes the symmetry of the new phase. Hence, the problem of solving the first bifurcation equation reduces to determining the eigenvalues and eigenvectors of the excluded volume "operator" $\mathcal{E}(\Omega, \Omega')$.

In general, there will be a degenerate set of eigenvectors corresponding to the most negative eigenvalue. In order to determine the nature of the new phase, more information is needed. This information can be found in the second-order bifurcation equation given by

$$\begin{aligned}\psi_2(\Omega) = -\frac{1}{8\pi^2}\Bigg[& n_0 \int d\Omega'\,\mathcal{E}\left(\Omega,\Omega'\right)\psi_2\left(\Omega'\right) + n_1 \int d\Omega'\,\mathcal{E}\left(\Omega,\Omega'\right)\psi_1\left(\Omega'\right) \\ & - \frac{1}{2}n_0^2\left\{\left(\int d\Omega'\mathcal{E}\left(\Omega,\Omega'\right)\psi_1\left(\Omega'\right)\right)^2 - \frac{1}{8\pi^2}\int d\Omega'\,\left(\int d\Omega''\,\mathcal{E}\left(\Omega',\Omega''\right)\psi_1\left(\Omega''\right)\right)^2\right\}\Bigg].\end{aligned} \tag{4.19}$$

This is an equation for ψ_2 with n_0 known and ψ_1 known up to second order in ϵ.

Let us take a closer look at the excluded volume $\mathcal{E}(\Omega, \Omega')$ of two particles, which is the volume that one particle with orientation Ω excludes to a second particle with orientation Ω'. For hard rectangular rods with restricted orientations, as in the Zwanzig model [35], the excluded volume is known exactly and given by

$$\mathcal{E}(s, s') = e_{\parallel}\delta_{s,s'} + e_{\perp}(1 - \delta_{s,s'}), \tag{4.20}$$

where $e_{\parallel}$ is the excluded volume of two particles orientated parallel with respect to each other, and $e_{\perp}$ is the excluded volume of two perpendicular particles. If the dimensions of these particles are known, these excluded volumes can be easily calculated.

The excluded volume of two spherocylinders that are free to rotate is also well-known [36] and given by

$$\mathcal{E}(\gamma) = 2L^2D|\sin\gamma(\Omega,\Omega')| + 8v_0, \tag{4.21}$$

where $v_0 = \pi LD^2/4 + \pi D^3/6$ is the volume of a spherocylinder, and $\gamma = \arccos(\Omega \cdot \Omega')$ is the angle between the two spherocylinders.

The excluded volume of two banana-shaped particles with restricted orientations cannot be found exactly because of the non-convex shape of the particles, although a mixed analytical and numerical method does exist [37]. However, we can make use of the symmetry of both the excluded volume and the particles to find a basis of functions that the excluded volume can be expanded in. This will be discussed in Chapter 6 and 7.

This approach can be extended to systems where spatial modulations are present, such as in the splay-bend phase discussed in Section 3.4.3. Since the one-particle distribution is now dependent on both the position and orientation, we cannot use the approximation from Section 4.3. That means the Mayer function from Eq. (4.9) needs to be used instead of the excluded volume, which complicates the calculation.

CHAPTER 5

Representation theory

In this chapter, an introduction to group theory and the closely-related representation theory will be given. Groups are important because they describe the symmetries of a physical system. This will turn out to be useful when describing the symmetries of particles of different shapes and the excluded volume of two particles. This chapter is broadly based on the first four chapters of Ref. [38].

5.1 Group theory

A set of elements forms a group if it satisfies the following four requirements:

1. Closure: The product of any two elements is an element of the group itself.
2. Associativity: For all A, B, and C in the group, one has $(AB)C = A(BC)$.
3. Identity element: There exists an element E such that its product with any group element leaves that group element unchanged.
4. Inverse element: For every element A there exists an element A^{-1} such that $AA^{-1} = E$.

5.1.1 Symmetry operations versus permutations

A simple example of a group is the permutation group S_3 of three elements 1, 2, 3. These three elements (1, 2, 3) can be permuted in six different ways

$$\begin{aligned} E &= \begin{pmatrix} 1 & 2 & 3 \end{pmatrix} \quad A = \begin{pmatrix} 2 & 1 & 3 \end{pmatrix} \quad B = \begin{pmatrix} 1 & 3 & 2 \end{pmatrix} \\ C &= \begin{pmatrix} 3 & 2 & 1 \end{pmatrix} \quad D = \begin{pmatrix} 3 & 1 & 2 \end{pmatrix} \quad F = \begin{pmatrix} 2 & 3 & 1 \end{pmatrix} \end{aligned} \tag{5.1}$$

This group is identical to the symmetry group of an equilateral triangle, which is known as the dihedral group D_3. Consider an equilateral triangle with three corners 1, 2 and 3. There are six transformations that leave this triangle invariant. These symmetry operations are

$$\begin{aligned} E &= \text{Identity}, \\ A &= \text{Rotation of } 180^\circ \text{ around the median through 3}, \\ B &= \text{Rotation of } 180^\circ \text{ around the median through 1}, \\ C &= \text{Rotation of } 180^\circ \text{ around the median through 2}, \\ D &= \text{Right rotation of } 270^\circ \text{ around the origin}, \\ F &= \text{Left rotation of } 270^\circ \text{ around the origin}. \end{aligned} \tag{5.2}$$

Each symmetry operation is called an element of the group.

There exists a difference between a concrete geometrical realisation such as D_3 and the abstract underlying group like S_3. However, these two groups are isomorphic, which means that there is a one-to-one correspondence between the elements of these groups. Isomorphic groups have the same properties. That means one does not have to distinguish between the two if one is interested in the group structure and not the specific elements.

It is convenient to write the products of group elements in a multiplication table. The products of the elements of S_3 are shown in Table 5.1, which will be helpful when multiplying elements later.

Table 5.1: Multiplication table of the permutation group S_3

	E	A	B	C	D	F
E	E	A	B	C	D	F
A	A	E	D	F	B	C
B	B	F	E	D	C	A
C	C	D	F	E	A	B
D	D	C	A	B	F	E
F	F	B	C	A	E	D

5.1.2 Subgroups and cosets

Subgroups are a set of elements in a group that form a group themselves. Each group has at least two subgroups, the group itself and the group containing only the identity element. S_3 has six subgroups

$$\begin{array}{ccc} E & (E,A) & (E,B) \\ (E,C) & (E,D,F) & (E,A,B,C,D,F) \end{array} \tag{5.3}$$

Given an element g of G, the left cosets of H in G are the sets obtained by multiplying each element of H by a fixed element g of G (where g is the left factor). In symbols these are,

Consider now a group G with elements g and a subgroup H with elements h. The left cosets of H in G are the sets obtained by multiplying each element of H with a fixed element g of G from the left. The left coset of H with representative g is then defined as

$$gH = \{gh \,|\, h \in H\}\,. \tag{5.4}$$

Right cosets can be defined in a similar way, but now by multiplying each element of H from the right with a fixed element g. A left coset is not necessarily a subgroup of G, it is only a subgroup if g is an element of H. Two cosets are multiplied together by multiplying the constituent elements of each coset in the right order. Two left cosets either contain exactly the same elements or have no elements in common. This means that the left cosets of a subgroup partition the group. Two elements that are in the same left coset are related by an equivalence relation.

An example of an equivalence relation is when two elements of a group are conjugate. Consider two elements a and b in group G. If there is an element $c \in G$ for which $b = c^{-1}ac$, then a and

b are considered conjugate. The equivalence classes corresponding to this equivalence relation are called conjugacy classes.

Let us look at an example with $H = E, A$ as a subgroup of S_3. Using the products written in the multiplication table in Table 5.1, we can determine the left cosets of H in S_3

$$\begin{aligned} E(E,A) &= E,A \quad A(E,A) = A,E \quad B(E,A) = B,F \\ C(E,A) &= C,D \quad D(E,A) = D,C \quad F(E,A) = F,B. \end{aligned} \tag{5.5}$$

That leaves us with three distinct left cosets

$$(E,A), \quad (B,F), \quad (C,D), \tag{5.6}$$

of which only the first is a subgroup of S_3.

5.2 Representation theory

Closely related to group theory, there is representation theory. Representation theory aims to describe abstract algebraic structures, such as groups, in terms of linear transformations of vector spaces. In the case of groups, elements of a group are represented by invertible matrices. Similarly, the group operations are represented by matrix operations. In this way, abstract problems in group theory are reduced to linear algebra problems, for which there exist well-known methods of solving them.

Representations of groups are important because they describe how the solutions of equations are affected by the symmetry of a physical system. Representation theory has applications in mathematics, but also in quantum chemistry and physics. In crystallography, it is used to determine the degeneracy and the symmetries of the split energy levels in a crystal. It can also be used to the derive the selection rules in spectroscopy, or to construct the spin representations of the Lorentz group.

5.2.1 Matrix representation

Going back to our example of S_3, we can assign a matrix $R(X)$ to each element X of the abstract group such that it satisfies the multiplication table of Table 5.1. An example of such a set of matrices is

$$\begin{gathered} E = \begin{pmatrix} 1 & 0 \\ 0 & 1 \end{pmatrix} \qquad A = \begin{pmatrix} 1 & 0 \\ 0 & -1 \end{pmatrix} \qquad B = \begin{pmatrix} -\frac{1}{2} & \frac{\sqrt{3}}{2} \\ \frac{\sqrt{3}}{2} & \frac{1}{2} \end{pmatrix} \\ C = \begin{pmatrix} -\frac{1}{2} & -\frac{\sqrt{3}}{2} \\ -\frac{\sqrt{3}}{2} & \frac{1}{2} \end{pmatrix} \quad D = \begin{pmatrix} -\frac{1}{2} & \frac{\sqrt{3}}{2} \\ -\frac{\sqrt{3}}{2} & -\frac{1}{2} \end{pmatrix} \quad F = \begin{pmatrix} -\frac{1}{2} & -\frac{\sqrt{3}}{2} \\ \frac{\sqrt{3}}{2} & -\frac{1}{2} \end{pmatrix}. \end{gathered} \tag{5.7}$$

However, these representations are not unique. Another set of matrices can be generated via an equivalence transformation $UR(X)U^{-1}$ with U a unitary matrix. One could also generate a new representation by combining one or more representations as

$$\begin{pmatrix} R(X) & \mathcal{O} \\ \mathcal{O}^T & R'(X) \end{pmatrix}, \tag{5.8}$$

where $\mathcal{O}$ is a matrix of zeros and $R'(x)$ can be equal to $R(X)$ or a different representation.

5.2.2 Irreducible representations

If all matrices in the representation of a group can be written in block form (like in Eq. (5.8)) by one and the same equivalence transformation, that representation is reducible. Otherwise it is irreducible. An irreducible representation cannot be broken down into representations of lower dimensionality.

The permutation group S_3 has three irreducible representations $\mathrm{A}_1, \mathrm{A}_2$ and E. The first two are one-dimensional representations, where A_1 is known as the trivial representation, which is always 1, and A_2 as the sign representation, which is ± 1 depending on the sign of the permutation. The representation E is two-dimensional and therefore a 2×2 matrix. Note the difference in notation between the symmetry operation E and the irreducible representation E. The irreducible representations for the six permutations are given by

	E	A	B
Γ_{A_1}	(1)	(1)	(1)
Γ_{A_2}	(1)	(-1)	(-1)
Γ_{E}	$\begin{pmatrix} 1 & 0 \\ 0 & 1 \end{pmatrix}$	$\begin{pmatrix} 1 & 0 \\ 0 & -1 \end{pmatrix}$	$\begin{pmatrix} -\frac{1}{2} & \frac{\sqrt{3}}{2} \\ \frac{\sqrt{3}}{2} & \frac{1}{2} \end{pmatrix}$
	C	D	F
Γ_{A_1}	(1)	(1)	(1)
Γ_{A_2}	(-1)	(1)	(1)
Γ_{E}	$\begin{pmatrix} -\frac{1}{2} & -\frac{\sqrt{3}}{2} \\ -\frac{\sqrt{3}}{2} & \frac{1}{2} \end{pmatrix}$	$\begin{pmatrix} -\frac{1}{2} & \frac{\sqrt{3}}{2} \\ -\frac{\sqrt{3}}{2} & -\frac{1}{2} \end{pmatrix}$	$\begin{pmatrix} -\frac{1}{2} & -\frac{\sqrt{3}}{2} \\ \frac{\sqrt{3}}{2} & -\frac{1}{2} \end{pmatrix}$

(5.9)

A reducible representation of S_3 can then be written as a linear combination of irreducible representations

$$\Gamma_R = \bigoplus_{\lambda} \Gamma_\lambda, \tag{5.10}$$

where $\lambda \in \{\mathrm{A}_1, \mathrm{A}_2, \mathrm{E}\}$ labels the irreducible representations of S_3. This shows that the irreducible representations of a symmetry group form a complete set of functions to describe the symmetry of an object belonging to that symmetry group. In solving a physical problem, one often has a matrix describing the properties of a system (such as the Hamiltonian). The irreducible representations then describe how a set of eigenvectors transforms and the way in which they correspond to distinct eigenvalues. The fact that a reducible representation can be split into several irreducible representations indicates that a symmetry is broken. However, group theory does not give us any information on the eigenvalues nor their ordering. It only describes the degeneracies of the eigenvalues and the symmetries of the eigenvectors.

5.3 Discrete symmetries

The symmetries of molecules or colloidal particles can be described by point groups [39]. Point groups are mathematical groups of symmetry operations that have a fixed point in common. For the sake of simplicity, let us now focus on describing particles whose body-mounted axes $\boldsymbol{m}_1, \boldsymbol{m}_2$,

and $\boldsymbol{m}_3$ can point in a restricted number of orientations, namely parallel to the Cartesian axes x, y, or z. In this case, we only consider point groups that contain discrete point symmetries.

5.3.1 Octahedral point group

The geometrical object with the highest symmetry is a cube, which is described by the rotational octahedral group O, which consists of 24 symmetry operations (rotations) of the cube that rotate the cube onto itself, and are thus orientation-preserving. This group is isomorphic to the symmetric group S_4 consisting of the 24 permutations of the four body-diagonals of a cube. The symmetry group O is the concrete geometrical representation, while the symmetric group S_4 is the abstract underlying group, but their properties are the same and hence the properties of the groups are equivalent. These 24 symmetry operations also correspond to the 24 ways in which one can rotate a particle of any symmetry. Not all of these rotations will lead to the same orientation of a particle, depending on the symmetry of the particle.

The 24 symmetry operations of a cube are divided into five conjugacy classes:

1. E with the identity operation,
2. $8C_3$ with the 8 rotations by 120° around a 3-fold axis,
3. $3C_2$ with the 3 rotations by 180° around a 2-fold axis,
4. $6C_4$ with the 6 rotations by 90° around a 4-fold axis,
5. $6C_2'$ with the 6 rotations by 180° around a 2-fold axis.

In Fig. 5.1(a), the rotation axes of a cube are shown.

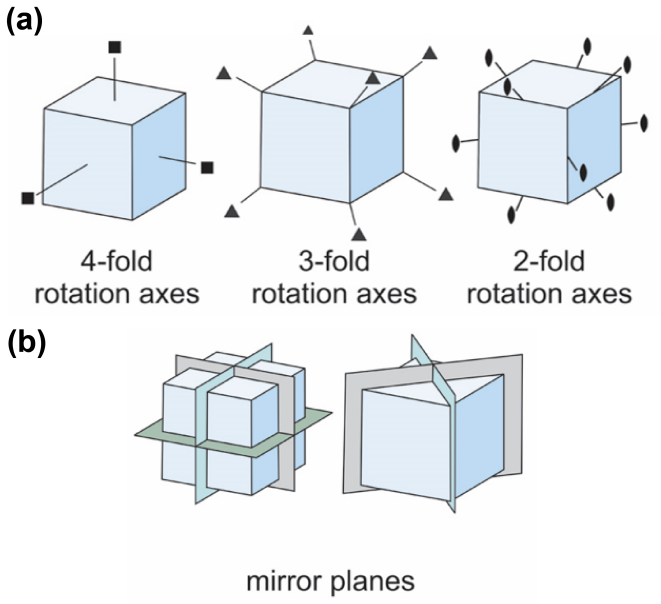

Figure 5.1: The symmetry axes and planes of a cube with octahedral symmetry described by the full octahedral point group O_h. Figure adapted from Ref. [40].

However, as shown in Fig. 5.1(b), a cube also has several horizontal, vertical and diagonal mirror planes and a center of inversion. The point group that contains the full symmetry of a cube is the full octahedral group O_h. In addition to the identity operation and the 23 rotations in the rotational octahedral group O, the O_h group also contains the 24 inversions of the elements of O that are divided into five other conjugacy classes:

1. I with the spatial inversion,

2. $6S_4$ with the 6 rotoreflections by 90°,

3. $8S_6$ with the 8 rotoreflections by 60°,

4. $3\sigma_h$ with the 3 reflections in a plane perpendicular to a 4-fold axis,

5. $6\sigma_d$ with the 6 reflections in a plane perpendicular to a 2-fold axis,

where a rotoreflection is a combination of a rotation and a reflection.

O_h is a direct product of the rotational octahedral group O and the cyclic group of order 2 Z_2, i.e. $O_h = O \times Z_2$. Here, Z_2 contains two elements, the identity E and the spatial inversion I. Hence, any element $p \in O_h$ is either of the form g or Ig, where $g \in O$. We can therefore label every element p as $(g, \pm 1)$, with 1 for the identity E and -1 for the inversion I.

5.3.2 Irreducible representations of the octahedral point group

Since every element of O_h can be written as a product of an element of O and an element of Z_2, we only need to know the irreducible representations of O. The number of irreducible representations is equal to the number of conjugacy classes, so O has five irreducible representations. These irreducible representations are the trivial representation A_1, the sign representation A_2, the two-dimensional representation E, the standard representation T_1, and the product of the standard and sign representations T_2. The label A indicates that the irreducible representation is one-dimensional and non-degenerate, E corresponds to a two-dimensional and doubly-degenerate representation and T indicates that the representation is three-dimensional and triply-degenerate. This information is summarized in Table 5.2.

Table 5.2: An overview of the five irreducible representations of the point group O, and the corresponding dimensionality and degeneracy.

Irreducible representation	Label	Dimensionality	Degeneracy
Trivial representation	A_1	1	1
Sign representation	A_2	1	1
Two-dimensional representation	E	2	2×2
Standard representation	T_1	3	3×3
Product of standard and sign representations	T_2	3	3×3
Total		10	24

The irreducible representations of O_h are then determined by taking the tensor product of the irreducible representations of O with the irreducible representations of Z_2. Z_2 has two one-dimensional irreducible representations, namely A which is always 1, and B which is -1 for rotations around the principle axis and +1 otherwise. The point group O_h therefore has 10 irreducible representations for 48 symmetry operations.

Using the method from Ref. [41], where each permutation of S_4 is decomposed into permutations of two adjacent objects for which we can determine the matrix form of the irreducible representation, the five irreducible representations $R^\lambda(g)$ can be found for every element g in O, where $\lambda \in A_1$, A_2, E , T_1, T_1 labels the irreducible representation.

5.3.3 C_{2v} point group

Another point group that will be very important in the remainder of this thesis, is the C_{2v} point group. This point group describes the symmetry of a banana-shaped particle, as well as the symmetry of a water molecule as shown in Fig. 5.2. It contains four elements:

1. E with the identity operation,
2. C_2 with the rotation by 180° around a 2-fold axis,
3. $\sigma_v(xz)$ with the reflection in the xz-plane,
4. $\sigma_v(yz)$ with the reflection in the yz-plane.

The C_{2v} point group contains reflections in addition to a rotation and the identity. It is therefore only a subgroup of O_h and not of O. Since reflections and inversions of particles are unphysical in a liquid crystal, you might think that we only need to consider rotations. However, the fact that C_{2v} contains reflections does mean we have to work with the full octahedral group O_h in calculating cosets.

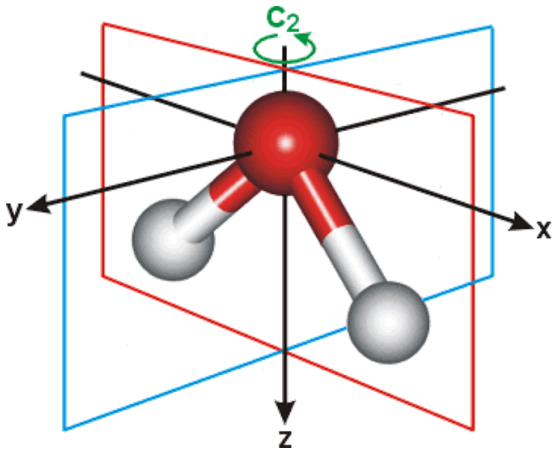

Figure 5.2: The two-fold rotation axis and the two mirror planes of a water molecule with C_{2v} symmetry. A banana-shaped particle also belongs to this symmetry group and has the same symmetries as a water molecule. Figure from Ref. [42].

CHAPTER 6

Rods with restricted orientations

In this chapter we will consider a simple model of a liquid crystal of hard rod-like particles. These particles can be treated as rectangular bars of length L and thickness D such that the rods have dimensions $L \times D \times D$. We can simplify this model even more by only considering three possible orientations where the long axis of the particles is aligned with one of the x, y and z-axes. In this section, we will look at three different approaches to describe the phases of a discrete model of a liquid crystal of straight hard rods.

6.1 The Zwanzig model

In 1963, Zwanzig [35] verified Onsager's prediction of a first-order phase transition in a system of long thin rods [4] using this simple model of rods with restricted orientations. The derivation below is inspired by Zwanzig's method and roughly based on Ref. [43].

Consider the Helmholtz free energy of these rods in a volume V and temperature T within the second virial approximation given by

$$\frac{\beta F}{V} = \sum_{\alpha \in \{x,y,z\}} \rho_\alpha \left(\log(\rho_\alpha \mathcal{V}) - 1\right) + \sum_{\alpha,\alpha' \in \{x,y,z\}} B_{\alpha\alpha'} \rho_\alpha \rho_{\alpha'}, \tag{6.1}$$

where ρ_α is the density of particles with orientation $\alpha \in \{x, y, z\}$. Here, $\mathcal{V}$ is the thermal volume that we take to be $\mathcal{V} = L^2 D$ for convenience, and $B_{\alpha\alpha'}$ is the second virial coefficient for two particles with orientations α and α' respectively. The second virial coefficients are given by

$$B_{\alpha\alpha'} = -\frac{1}{2} \int d\boldsymbol{r} f_{\alpha\alpha'}(\boldsymbol{r}), \tag{6.2}$$

with $f_{\alpha\alpha'}(\boldsymbol{r})$ the Mayer function of two particles with orientations α and α' at a distance $\boldsymbol{r}$. The Mayer function gives -1 if the two particles overlap and 0 if they do not.

There are two situations possible. Either the two rods are aligned in a parallel way (see Fig. 6.1(a)) or the rods are perpendicular (see Fig. 6.1(b)). In the parallel case, the second virial coefficients B_{xx}, B_{yy}, and B_{zz} are equal to $B_\parallel$. In the perpendicular case, we have $B_{xy} = B_{yx} = B_{xz} = B_{zx} = B_{yz} = B_{zy} \equiv B_\perp$. Performing the integrals of $B_\parallel$ and $B_\perp$ explicitly over the whole space gives

$$B_\parallel = \frac{1}{2} \cdot 2L \cdot 2D \cdot 2D = 4LD^2 \tag{6.3}$$

$$B_\perp = \frac{1}{2} \cdot (L + D) \cdot (L + D) \cdot 2D = (L + D)^2 D \tag{6.4}$$

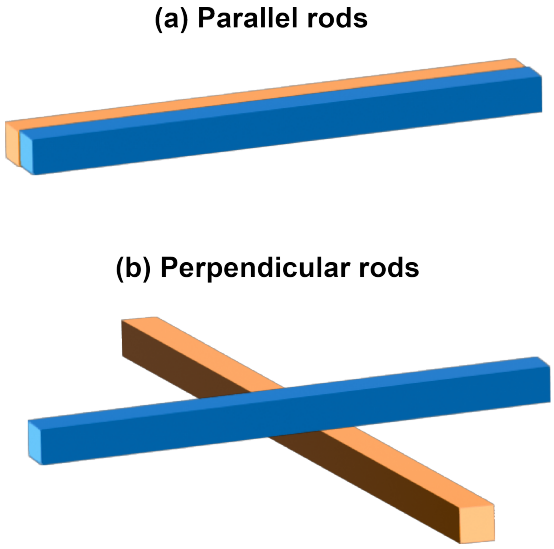

Figure 6.1: Two rods in (a) a parallel configuration and (b) a perpendicular configuration.

In the limit of needle-like particles where $L/D \to \infty$ and using L^2D as our unit of volume, we find $B_\parallel/(L^2D) \to 0$ and $B_\perp/(L^2D) \to 1$. Rewriting the free energy as a dimensionless free energy density f in terms of the dimensionless density $c_\alpha = L^2D\rho_a$ yields

$$f = \frac{\beta F L^2 D}{V} = \sum_{\alpha\in\{x,y,z\}} c_\alpha \left(\log(c_\alpha) - 1\right) + \sum_{\alpha\in\{x,y,z\}} \sum_{\alpha'\neq\alpha} c_\alpha c_{\alpha'}. \tag{6.5}$$

When this system transitions from an isotropic to a nematic phase, a symmetry is broken. We can manually include this symmetry breaking by introducing a scalar order parameter S. Writing the dimensionless density $\boldsymbol{c}$ in terms of the scalar order parameter gives

$$\boldsymbol{c} = \frac{c}{3}\begin{pmatrix} 1-S \\ 1-S \\ 1+2S \end{pmatrix}, \tag{6.6}$$

where c is the total dimensionless density $\rho L^2 D$ and we have chosen to break the symmetry in the z direction, such that the nematic director $\boldsymbol{n}$ is aligned with the z-axis. Now $S = 0$ corresponds to an isotropic phase, where $c_x = c_y = c_z = c/3$, and $S = 1$ corresponds to a nematic phase with $c_x = c_y = 0$ and $c_z = c$. Inserting $\boldsymbol{c}$ into Eq. (6.5) gives, after some rewriting,

$$\begin{aligned} f(c,S) = c\left(\log\left(\frac{c}{3}\right) - 1\right) + \frac{2c}{3}(1-S)\log(1-S) + \frac{c}{3}(1+2S)\log(1+2S) \\ + \frac{2c^2}{9}(1-S)^2 + \frac{4c^2}{9}(1+2S)(1-S). \end{aligned} \tag{6.7}$$

The system will arrange itself such that S minimizes the free energy at a given density c. Similar to the approach in Section 3.3.1, one can find the values of S that correspond to the minima of this system. The stability of these solutions can be investigated by looking at the sign of $\partial^2 f/\partial S^2$.

Following Ref. [43], one then finds an isotropic phase for $0 < c < c_I$, with c_I the density in the isotropic phase, and a nematic phase for $c > c_N$ with c_N the density of the nematic phase. For $c_I < c < c_N$, the isotropic phase with density c_I and the nematic phase with density c_N and

order parameter S_N are in coexistence. Solving for the three unknowns, we find [43]

$$c_I = 1.258, \tag{6.8}$$
$$c_N = 1.915, \tag{6.9}$$
$$S_N = 0.915. \tag{6.10}$$

6.2 Bifurcation analysis of rods with restricted orientations

6.2.1 Eigensystem of the excluded volume

The second approach is based on the eigenvectors and eigenvalues of the excluded volume matrix. We start from the free energy functional describing a spatially homogeneous phase in Eq. (4.15) and adapt it to this discrete case as

$$\frac{\beta\mathcal{F}[\psi]}{N} = \sum_{s=0}^{2} \psi(s)\left(\ln\psi(s) - 1\right) + \frac{1}{2}n\sum_{s=0}^{2}\sum_{s'=0}^{2}\mathcal{E}(s,s')\psi(s)\psi(s') + \ln(n\mathcal{V}), \tag{6.11}$$

where the allowed orientations are now labeled by s which runs from 0 to 2 for convenience.

The excluded volume of a liquid crystal of rods with restricted orientations can be written as a 3×3 matrix

$$\mathcal{E}_{rods} = \begin{pmatrix} e_\parallel & e_\perp & e_\perp \\ e_\perp & e_\parallel & e_\perp \\ e_\perp & e_\perp & e_\parallel \end{pmatrix}, \tag{6.12}$$

where $e_\parallel$ is the excluded volume of two parallel rods and $e_\perp$ that of two perpendicular rods. The eigenvectors and their corresponding eigenvalues are given in Table 6.1. The first eigenvector shows the symmetry of the isotropic phase. There is no preferred axis which is characteristic of an isotropic phase without orientational order. The second and third eigenvector are degenerate and both correspond to a nematic phase. In the second eigenvector, the z component is different from the x and y component, suggesting z-axis is the preferred axis. This is characteristic of a uniaxial nematic phase where the long axis of the particles points in the z direction. The third eigenvector also has the z-axis as the preferred axis, but now the x and y components are not equal. Hence, this eigenvector corresponds to a biaxial nematic phase with orientational ordering in two dimensions.

Table 6.1: The eigenvalues and eigenvalues of the excluded volume matrix describing a liquid crystals of rods with restricted orientations.

	Isotropic	Uniaxial nematic	Biaxial nematic
Eigenvalues	$e_\parallel + 2e_\perp$	$e_\parallel - e_\perp$	$e_\parallel - e_\perp$
Eigenvectors	$\begin{pmatrix} 1 \\ 1 \\ 1 \end{pmatrix}$	$\begin{pmatrix} -1 \\ -1 \\ 2 \end{pmatrix}$	$\begin{pmatrix} -1 \\ 1 \\ 0 \end{pmatrix}$

6.2.2 Bifurcation analysis of rods with restricted orientations

The third method is based on bifurcation analysis. The excluded volume of two straight rods with restricted orientations can be written in a different way as

$$\begin{aligned}\mathcal{E}(s,s') &= e_{\parallel}\,\delta(s,s') + e_{\perp}\,(1-\delta(s,s')) \\ &= (e_{\parallel}-e_{\perp})\,\delta(s,s') + e_{\perp},\end{aligned} \tag{6.13}$$

where s again labels the orientations x, y, z. Introducing the dimensionless number density $\eta = n\,(e_{\perp} - e_{\parallel})$ and substituting this in Eq. (6.11) yields

$$\frac{\beta\mathcal{F}[\psi]}{N} = \sum_{s=0}^{2}\psi(s)\,(\ln\psi(s)-1) - \frac{1}{2}\eta\sum_{s=0}^{2}\sum_{s'=0}^{2}\delta_{s,s'}\psi(s)\psi(s') + \frac{1}{2}ne_{\perp} + \ln(n\mathcal{V}). \tag{6.14}$$

Instead of determining the first bifurcation equation again, we can use the general bifurcation equation in Eq. (4.18) if we make the following changes:

1. replacing the integrations over Ω by summations over s;
2. replacing the factor 8π by the number 3 which represents the "volume" of the discrete orientation space;
3. replacing the excluded volume by the reduced excluded volume $-\delta_{s,s'}$;
4. replacing the number density n by the dimensionless density η.

The first bifurcation equation is then given by

$$\psi_1(s) = \frac{\eta_0}{3}\sum_{s=0}^{2}\delta_{s,s'}\psi_1(s'). \tag{6.15}$$

Although in this simple case the eigenfunctions, and thus a complete set of functions of the excluded volume are known, we will use a more systematic approach. This will be useful when considering liquid crystals of banana-shaped particles. The symmetry of the excluded volume of rods with restricted orientations can described by the permutation group S_3. However, it is also possible to work with a subgroup of S_3, namely the group of cyclic permutations of three objects C_3.

The point group C_3 has two irreducible representations, the one-dimensional trivial representation A and the two-dimensional representation E. However, if we allow for complex numbers, the two-dimensional representation can be reduced to two complex numbers. That gives

$$\begin{aligned}\phi_0 &= 1, \\ \phi_1 &= e^{\frac{2\pi i}{3}}, \\ \phi_2 &= e^{\frac{4\pi i}{3}},\end{aligned} \tag{6.16}$$

or written as functions of the orientation s,

$$\phi_k(s) = e^{\frac{2\pi i}{3}ks}, \quad \text{with } k = 0, 1, 2. \tag{6.17}$$

These functions form a complete orthogonal set under the inner product defined by

$$\langle\phi_i|\phi_j\rangle = \sum_{s=0}^{2}\phi_i^*(s)\phi_j(s) = 3\delta_{s,s'}, \tag{6.18}$$

and can therefore be used in the expansion of the reduced excluded volume

$$\delta_{s,s'} = \frac{1}{3}\sum_{k=0}^{2}\phi_k(s)\phi_k^*(s'). \tag{6.19}$$

Every $\phi_k(s)$ is an eigenfunction of the reduced excluded volume with eigenvalue 1. Since the first eigenfunction ϕ_0 is a constant, it is related to the isotropic distribution function ψ_0. The bifurcation eigenfunction is thus a linear combination of the other two eigenfunctions

$$\psi_1(s) = c_1\phi_1(s) + c_2\phi_2(s). \tag{6.20}$$

Inserting this into the first bifurcation equation in Eq. (6.15) gives

$$\begin{aligned}
\psi_1(s) &= \frac{\eta_0}{3}\sum_{s=0}^{2}\delta_{s,s'}\left(c_1\phi_1(s') + c_2\phi_2(s')\right) && (6.21)\\
&= \frac{\eta_0}{3}\left(c_1\phi_1(s) + c_2\phi_2(s)\right) && (6.22)\\
&= \frac{\eta_0}{3}\psi_1(s). && (6.23)
\end{aligned}$$

This fixes the bifurcation density at $\eta_0 = 3$. We now know when the bifurcation happens, but not what happens since the expansion coefficients c_1 and c_2 are undetermined. The expansion coefficients can be determined in two ways: either by fitting the bifurcation eigenfunction to two different numerical values of the excluded volume of two particles in different orientations, or by exploiting the second-order bifurcation equation. Using the latter method, following Ref. [34], we find three solutions for each expansion coefficient labeled by $n = 0, 1, 2$,

$$\begin{aligned}
c_1^{(n)} &= \frac{-2\eta_1}{9}e^{\frac{2\pi i}{3}n} && (6.24)\\
c_2^{(n)} &= \frac{-2\eta_1}{9}e^{\frac{4\pi i}{3}n}. && (6.25)
\end{aligned}$$

This yields three possible bifurcation eigenfunctions, labeled by $n = 0, 1, 2$, are

$$\begin{aligned}
\psi_1^{(n)}(s) &= \frac{-2\eta_1}{9}\left(e^{\frac{2\pi i}{3}(n-s)} + e^{\frac{4\pi i}{3}(n-s)}\right)\\
&= \frac{-2\eta_1}{9}\left(\phi_1(n)\phi_1^*(s) + \phi_2(n)\phi_2^*(s)\right)\\
&= \frac{-2\eta_1}{9}\left(3\delta_{n,s} - \phi_0(n)\phi_0^*(s)\right)\\
&= \frac{-2\eta_1}{9}\left(3\delta_{n,s} - 1\right), && (6.26)
\end{aligned}$$

where we have used the expansion of the reduced excluded volume of Eq. (6.19) in going from the second to third line.

We can see that the bifurcating solutions are symmetric around n, which we can now recognize as the ordering axis. The three solutions for the three possible ordering axes x, y, and z reflect that the axes are all equivalent. The solutions are therefore characteristic of a uniaxial nematic phase, which means that the bifurcation we have been studying is an isotropic to nematic phase transition. Most of the conclusions in this section follow from the properties of the reduced excluded volume. This illustrates why the problem of studying the bifurcation can be reduced to knowing the eigenfunctions of the excluded volume.

6.2.3 Connection to Landau theory

The combination of density functional theory and bifurcation analysis shows some agreement with Landau-de Gennes theory. The analogy can be found from the expansion of the distribution function $\psi(s)$ in terms of the eigenfunctions $\phi_k(s)$

$$\psi(s) = \sum_{k=0}^{2} c_k \phi_k(s). \tag{6.27}$$

The distribution function $\psi(s)$ is normalized as

$$\sum_{s=0}^{2} \psi_k(s) = \sum_{s=0}^{2} \phi_0(s)\psi_k(s) = 1, \tag{6.28}$$

where we can insert $\phi_0(s)$ since it has value 1 for every orientation s. Using the definition of the inner product in Eq. (6.18) and the fact that $\psi(s)$ is linear in $\phi_k(s)$, we can calculate

$$\begin{aligned}
\langle \phi_0 | \psi \rangle &= \sum_{s=0}^{2} \phi_0^*(s)\psi(s) \\
&= \sum_{s=0}^{2} \sum_{k=0}^{2} c_k \phi_0^*(s)\phi_k(s) \\
&= \sum_{k=0}^{2} c_k \cdot 3\,\delta(0,k) \\
&= 3c_0.
\end{aligned} \tag{6.29}$$

Hence, the normalization of $\psi(s)$ leads to the following constraint on the expansion coefficients

$$c_0 = \frac{1}{3}, \tag{6.30}$$

with c_1 and c_2 as free parameters. Since the isotropic phase is characterized by $c_0 = \frac{1}{3}$ and $c_1 = c_2 = 0$, the set of expansion coefficients c_1 and c_2 can be used as order parameters in the expansion of the free energy. Inserting the expansion of ψ in terms of c_1 and c_2 into the free energy expansion of Eq. (6.14), we find up to third order in c_1 and c_2 [34]

$$\frac{\beta\mathcal{F}}{N} = \frac{\beta\mathcal{F}_0}{N} + \frac{3}{2}(3-\eta)\sum_{k=1}^{2} c_k^* c_k - \frac{3}{2}\sum_{k=1}^{2}\sum_{k'=1}^{2}\sum_{k''=1}^{2} c_k c_{k'} c_{k''}\,\delta\left((k+k') \bmod d, d-k''\right) + \ldots. \tag{6.31}$$

The bifurcation density can be found from the quadratic term, namely $\eta = 3$, as we have seen before. The main difference with the Landau expansion of Section 3.4 is that the expansion parameters used here contain microscopic information about the particles and their interactions, while the expansion coefficients in de extended Landau-de Gennes theory do not.

Minimizing the free energy with respect to the order parameters c_k, one recovers the uniaxial nematic solution from Eq. (6.26). In this way, one obtains the same information about the bifurcation as in Section 6.2.2 with the two bifurcation equations. However, with this method the free energy is expanded at fixed density. The expansion parameter ϵ from Section 6.2.2 is a much better measure of the distance to the bifurcation. Therefore, this approach of applying bifurcation analysis to the functional needs a more complex investigation than applying bifurcation analysis to the stationarity equations.

6.3 Aligned rods with smectic order

Up until now, we have assumed that the phases of the liquid crystal we are considering are spatially homogeneous. However, we know that for example liquid crystals of banana-shaped particles also exhibit spatial modulations, such as the splay-bend phase $\mathrm{Sm_{SB}}$. In this section, we will apply density functional theory to a liquid crystal of cylinders with length L and diameter D aligned in the z direction with smectic order.

The free energy functional for a system of hard aligned cylinders in the Onsager approximation, allowing for spatially inhomogeneous phases, is given by

$$\begin{aligned}\beta\mathcal{F}[\rho] &= \beta\mathcal{F}_{id}[\rho] + \beta\mathcal{F}_{ex}[\rho] \\ &= \int d\boldsymbol{r}\, \rho(\boldsymbol{r}) \Big(\ln[\rho(\boldsymbol{r})\mathcal{V}] - 1 \Big) - \frac{1}{2} \int d\boldsymbol{r} \int d\boldsymbol{r}'\, f(\boldsymbol{r}, \boldsymbol{r}')\rho(\boldsymbol{r})\rho(\boldsymbol{r}'),\end{aligned} \tag{6.32}$$

with $\mathcal{V}$ the thermal volume and where the Mayer function for two parallel cylinders is explicitly given by

$$f(\boldsymbol{r}) = -\Theta(L - |z|)\, \Theta(D - \sqrt{x^2 + y^2}), \tag{6.33}$$

where Θ is the Heaviside step function with value 0 for negative arguments and 1 for positive arguments.

To describe the smectic order of this system, we are interested in changes in the spatial density. These instabilities in the density correspond to points in space where the structure factor diverges. We know from Ornstein-Zernike theory [44] that the structure factor is given by

$$S(\boldsymbol{q}) = \frac{1}{1 - \rho\hat{c}(\boldsymbol{q})}, \tag{6.34}$$

with $\boldsymbol{q}$ the wave vector, ρ the density and $\hat{c}(\boldsymbol{q})$ the Fourier transform of the direct correlation function

$$c(\boldsymbol{r}, \boldsymbol{r}') = -\frac{\delta\beta\mathcal{F}_{ex}[\rho]}{\delta\rho(\boldsymbol{r})\delta\rho(\boldsymbol{r}')} = f(\boldsymbol{r} - \boldsymbol{r}'), \tag{6.35}$$

which turns out to be equal to the Mayer function within the second virial approximation. The instability with respect to the density will occur at $\rho\hat{c}(\boldsymbol{q}) = \rho\hat{f}(\boldsymbol{q}) \to 1$. To study the instability, we have to determine the Fourier transform of the Mayer function

$$\hat{f}(\boldsymbol{q}) = -\int dx \int dy \int dz\, e^{i\boldsymbol{q}\cdot\boldsymbol{r}}\, \Theta(L - |z|)\, \Theta(D - \sqrt{x^2 + y^2}). \tag{6.36}$$

Changing to polar coordinates s, ϕ, z gives

$$\begin{aligned}\hat{f}(\boldsymbol{q}) &= -\int dz \int ds \int d\phi\, s\, e^{iq_\parallel z}\, e^{iq_\perp s\cos\phi}\, \Theta(L - |z|)\, \Theta(D - s) \\ &= -\int_{-L}^{L} dz\, e^{iq_\parallel z} \cdot \int_0^D ds\, s \int_0^{2\pi} d\phi\, e^{iq_\perp s\cos\phi},\end{aligned} \tag{6.37}$$

where the wave vector $\boldsymbol{q}$ is split up into a part $q_\parallel$ parallel to the z-axis and a part $q_\perp$ perpendicular to the z-axis.

Calculating the first integral in the expression for $\hat{f}(\boldsymbol{q})$ yields

$$\int_{-L}^{L} dz\, e^{iq_\parallel z} = \frac{2sin(q_\parallel L)}{q_\parallel} = 2Lj_0(q_\parallel L), \tag{6.38}$$

with $j_0(x) = \frac{\sin(x)}{x}$ the zeroth spherical Bessel function.

For calculating the second part of $\hat{f}(\boldsymbol{q})$, we need the standard Bessel functions J_0 and J_1

$$J_0(x) = \frac{1}{2\pi}\int_0^{2\pi} d\phi\, e^{ix\cos\phi} \tag{6.39}$$

$$\begin{aligned}\frac{J_1(x)}{x} &= \int_0^1 dt\, t\, J_0(xt)\\ &= \frac{1}{2\pi}\int_0^1 dt\, t \int_0^{2\pi} d\phi\, e^{ixt\cos\phi}\\ &= \frac{1}{2\pi D^2}\int_0^D ds\, s \int_0^{2\pi} d\phi\, e^{ixs\cos\phi/D}.\end{aligned} \tag{6.40}$$

The second part of $\hat{f}(\boldsymbol{q})$ can be written in terms of the first standard Bessel function

$$\int_0^D ds\, s \int_0^{2\pi} d\phi\, e^{iq_\perp s\cos\phi} = \frac{2\pi D^2 J_1(q_\perp D)}{q_\perp D}. \tag{6.41}$$

That gives for the full Fourier transform of the Mayer function

$$\hat{f}(\boldsymbol{q}) = -4\pi L D^2\, j_0(q_\parallel L)\,\frac{J_1(q_\perp D)}{q_\perp D}. \tag{6.42}$$

Introducing the packing fraction $\eta = \frac{1}{4}\pi L D^2\rho$, the condition of instability becomes

$$-8\eta^* j_0(q_\parallel L)\,\frac{J_1(q_\perp^* D)}{\frac{1}{2}q_\perp^* D} = 1. \tag{6.43}$$

We are interested in the lowest density (or packing fraction η) for which the structure factor diverges. For all real $x \geq 0$

$$|j_0(x)| \leq 1, \tag{6.44}$$

$$\left|\frac{J_1(x)}{\frac{1}{2}x}\right| \leq 1, \tag{6.45}$$

such that the minimal value of η^* that meets the condition in Eq. (6.43) occurs at either $q_\parallel^* = 0$ or $q_\perp^* = 0$. Using the results from Ref. [33] we find two sets of solutions

$$\eta_\parallel^* = 0.575, \quad q_\parallel^* L = 4.493, \quad q_\perp^* D = 0; \tag{6.46}$$

$$\eta_\perp^* = 0.945, \quad q_\parallel^* L = 0, \quad q_\perp^* D = 5.136. \tag{6.47}$$

The second set of solutions, corresponding to transverse modulations (perpendicular to the preferred axis) occurs at an higher packing fraction than the first set of solutions, corresponding to spatial modulations along the preferred axis. Additionally, the perpendicular packing fraction $\eta_\perp^*$ is unphysical since it is above the close packing of cylinders η_{cp}. The packing fraction of closely packed cylinders in 3D is equal to the packing fraction of closely packed circles in 2D, which is given by

$$\eta_{cp} = \frac{\text{Area of circles inside hexagon}}{\text{Area of a hexagon of side length } D} = \frac{\frac{3\pi}{4}D^2}{\frac{3\sqrt{3}}{2}D^2} = \frac{\pi}{2\sqrt{3}} \approx 0.907. \tag{6.48}$$

For these reasons we can focus on the longitudinal modulations occurring at the bifurcation packing fraction $\eta_\parallel^*$. Assuming that the modulations of the average density ρ along the z-axis are periodic, we can expand the one-particle distribution function as

$$\rho(\boldsymbol{r}) = \rho\left(1 + \sum_{l=1}^{\infty} a_l \cos(lqz)\right), \tag{6.49}$$

with a_l the undetermined amplitudes. The bifurcation analysis can then be performed by following these steps:

1. Insert the expansion into the free energy functional from Eq. (6.32);
2. Expand the packing fraction η, the amplitudes a_l and the wave number q in orders of ϵ;
3. Solve the stationarity equations $\frac{\delta \mathcal{F}[\psi]}{\delta a_l} = 0$ for $l \geq 1$ and $\frac{\delta \mathcal{F}[\psi]}{\delta q} = 0$.

Using the results from Ref. [33], we find that for $\eta > \eta_0$ the ordered solution corresponding to the smectic phase, has a lower free energy than the disordered solution corresponding to the nematic phase. Furthermore, the phase transition occurring at the bifurcation point η_0 is a second-order phase transition.

CHAPTER 7

Banana-shaped particles with restricted orientations

7.1 Discrete orientations of a banana-shaped particle

After looking at a system of rods with restricted orientation, let us now consider a liquid crystal of banana-shaped particles with restricted orientations. The twelve distinguishable orientations of a particle with C_{2v} symmetry are shown in Fig. 7.1, where the capital letter labels the direction of the long axis $\boldsymbol{m}_2$ and the subscript labels the direction of the polar axis $\boldsymbol{m}_1$, see Fig. 2.1.

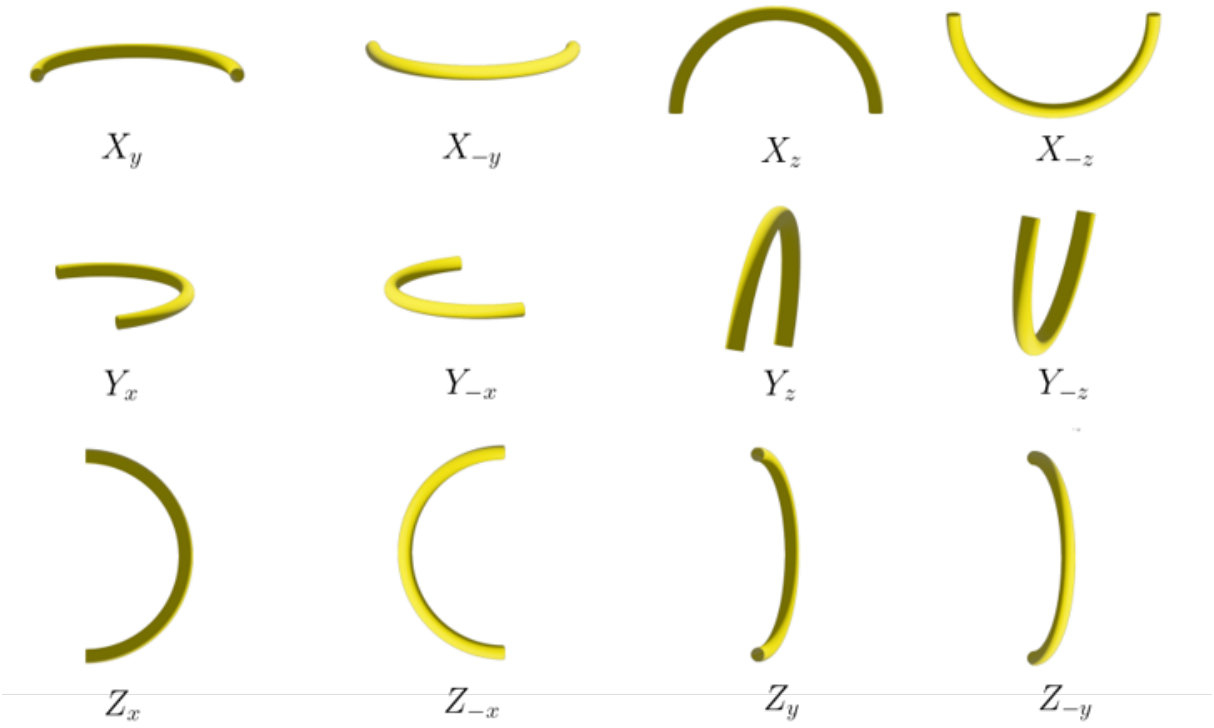

Figure 7.1: The twelve distinguishable orientations of a banana-shaped particle with C_{2v} symmetry.

The twelve orientations can be obtained by rotating the particle around the symmetry axes of a cube. Although there are 24 rotations in the rotational octahedral group O, not all of them lead to distinguishable orientations of the banana-shaped particle. In Table 7.1, the orientations of a particle are linked to the corresponding element of the point group O. The number in parentheses indicates in how many ways the orientation can be obtained.

Table 7.1: The orientations linked to the elements of O, with the number in parentheses indicating the number of ways the orientation can be realised.

Element of O	Orientation of a particle (number of ways)
E	Z_x (1)
$8C_3$	X_y (2), X_{-y} (2), Y_z (2), Y_{-z}(2)
$3C_2$	Z_x (1), Z_{-x} (2)
$6C_4$	Z_y (1), Z_{-y} (1), X_z (1), X_{-z} (1), Y_x (2)
$6C_2'$	Z_y (1), Z_{-y} (1), X_z (1), X_{-z} (1), Y_x (1), Y_{-x} (1)

7.2 The excluded volume of banana-shaped particles

We are interested in the excluded volume of two hard banana-shaped particles with restricted orientations. Let us first determine how many different excluded volumes exist. Consider the first particle to have orientation Z_x. The second particle can be in one of the twelve different orientations. Studying the excluded volumes of these two particles, we find seven different excluded volumes (see Table 7.2).

Table 7.2: The seven different excluded volumes linked to the orientation of the second particle. The first particle is in the Z_x orientation.

Orientation of 2$^{\text{nd}}$ particle	Excluded volume
Z_x	E_1
Z_{-x}	E_2
Z_y	E_3
Z_{-y}	E_3
Y_x	E_4
Y_{-x}	E_5
Y_z	E_6
Y_{-z}	E_6
X_y	E_6
X_{-y}	E_6
X_z	E_7
X_{-z}	E_7

Although the twelve orientations can be obtained using only the rotations of O, C_{2v} containes reflections and is therefore a subgroup of O_h and not O. That is why we need the full octahedral group to calculate the left cosets of C_{2v} in O_h. Since C_{2v} has four elements and O_h has 48, the full octahedral group is divided up into $|O_h|/|C_{2v}| = 48/4 = 12$ cosets, each with four equivalent elements. Here, the equivalence relation is that the symmetry operations corresponding to the four elements in each coset all result in the same orientation of the banana-shaped particle. The twelve distinguishable configurations of a banana-shaped particle are therefore isomorphic to

the set of left-cosets $\Gamma = O_h/C_{2v}$. The elements of Γ are denoted by γ.

The excluded volume of two banana-shaped particles with restricted orientations can be written as a 12×12 matrix with seven different excluded volumes, given by

$$\mathcal{E}_{bananas} = \begin{pmatrix} e_1 & e_2 & e_3 & e_3 & e_4 & e_5 & e_6 & e_6 & e_7 & e_7 & e_6 & e_6 \\ e_2 & e_1 & e_3 & e_3 & e_5 & e_4 & e_6 & e_6 & e_7 & e_7 & e_6 & e_6 \\ e_3 & e_3 & e_1 & e_2 & e_6 & e_6 & e_7 & e_7 & e_6 & e_6 & e_4 & e_5 \\ e_3 & e_3 & e_2 & e_1 & e_6 & e_6 & e_7 & e_7 & e_6 & e_6 & e_5 & e_4 \\ e_4 & e_5 & e_6 & e_6 & e_1 & e_2 & e_3 & e_3 & e_6 & e_6 & e_7 & e_7 \\ e_5 & e_4 & e_6 & e_6 & e_2 & e_1 & e_3 & e_3 & e_6 & e_6 & e_7 & e_7 \\ e_6 & e_6 & e_7 & e_7 & e_3 & e_3 & e_1 & e_2 & e_4 & e_5 & e_6 & e_6 \\ e_6 & e_6 & e_7 & e_7 & e_3 & e_3 & e_2 & e_1 & e_5 & e_4 & e_6 & e_6 \\ e_7 & e_7 & e_6 & e_6 & e_6 & e_6 & e_4 & e_5 & e_1 & e_2 & e_3 & e_3 \\ e_7 & e_7 & e_6 & e_6 & e_6 & e_6 & e_5 & e_4 & e_2 & e_1 & e_3 & e_3 \\ e_6 & e_6 & e_4 & e_5 & e_7 & e_7 & e_6 & e_6 & e_3 & e_3 & e_1 & e_2 \\ e_6 & e_6 & e_5 & e_4 & e_7 & e_7 & e_6 & e_6 & e_3 & e_3 & e_2 & e_1 \end{pmatrix}. \tag{7.1}$$

Unfortunately, the eigenvectors of this matrix are very complicated without using numerical values for the seven excluded volumes, which makes them not suitable to work with.

7.3 Symmetry breaking in the orientation distribution function

In this section, we will take a look at the orientation distribution function and how it depends on the symmetries of banana-shaped particles in a liquid crystal. We can manually break the symmetry in our system by placing the particles with their long axis $\boldsymbol{m}_2$ along the z-axis and with their polar axis $\boldsymbol{m}_1$ along the x-axis. Inspired by Section 6.1, the orientation distribution function ψ can now be manually constructed to either possess or break up-down, biaxial and polar symmetry

$$\begin{array}{ccc} \psi_{z,x} = \frac{1}{12}(1 + 2S + \alpha + \alpha') & \psi_{x,y} = \frac{1}{12}(1 - S + \beta') & \psi_{y,x} = \frac{1}{12}(1 - S + \gamma' + \gamma) \\ \psi_{z,-x} = \frac{1}{12}(1 + 2S - \alpha + \alpha') & \psi_{x,-y} = \frac{1}{12}(1 - S + \beta') & \psi_{y,-x} = \frac{1}{12}(1 - S + \gamma' - \gamma) \\ \psi_{z,y} = \frac{1}{12}(1 + 2S - \alpha') & \psi_{x,z} = \frac{1}{12}(1 - S - \beta') & \psi_{y,z} = \frac{1}{12}(1 - S - \gamma') \\ \psi_{z,-y} = \frac{1}{12}(1 + 2S - \alpha') & \psi_{x,-z} = \frac{1}{12}(1 - S - \beta') & \psi_{y,-z} = \frac{1}{12}(1 - S - \gamma'), \end{array} \tag{7.2}$$

where

- $S \neq 0$ breaks orientational symmetry,
- $\alpha \neq 0$ breaks up-down symmetry,
- $\alpha' \neq 0$ breaks biaxial symmetry in the z direction,
- $\beta' \neq 0$ breaks biaxial symmetry in the x direction,
- $\gamma \neq 0$ breaks polar symmetry,
- $\gamma' \neq 0$ breaks biaxial symmetry in the y direction.

By varying the parameters, the orientation distribution function describes

- an isotropic phase for $S = 0$, $\alpha = 0$ and $\alpha' = 0$,
- a nematic phase for $S > 0$, $\alpha = 0$ and $\alpha' = 0$,
- a biaxial phase for $S > 0$, $\alpha = 0$ and $\alpha' \neq 0$,
- a polar phase for $S > 0$, $\alpha \neq 0$ and $\alpha' = 0$,

with $\beta' = \gamma = \gamma' = 0$.

With an expression for the orientation distribution function, the order parameters can be calculated explicitly. The nematic tensor order parameter $\boldsymbol{Q}$ in this system is given by

$$\begin{aligned}
\boldsymbol{Q} &= \frac{3}{2}\left\langle \boldsymbol{m}_2^2 - \frac{1}{3}\mathbb{1}\right\rangle = \sum_{i,j\in\{x,y,z\}} \frac{3}{2}\left(\psi_{i,j} + \psi_{i,-j}\right)\hat{\boldsymbol{i}}\hat{\boldsymbol{i}} - \frac{1}{2}\mathbb{1} \\
&= \frac{3}{2}\Big(\left(\psi_{x,y} + \psi_{x,-y} + \psi_{x,z} + \psi_{x,-z}\right)\hat{\boldsymbol{x}}\hat{\boldsymbol{x}} + \left(\psi_{y,x} + \psi_{y,-x} + \psi_{y,z} + \psi_{y,-z}\right)\hat{\boldsymbol{y}}\hat{\boldsymbol{y}} \\
&\quad + \left(\psi_{z,x} + \psi_{z,-x} + \psi_{z,y} + \psi_{z,-y}\right)\hat{\boldsymbol{z}}\hat{\boldsymbol{z}}\Big) - \frac{1}{2}\mathbb{1} \\
&= \frac{3}{2}\left(\frac{1}{3}(1-S)\,\hat{\boldsymbol{x}}\hat{\boldsymbol{x}} + \frac{1}{3}(1-S)\,\hat{\boldsymbol{y}}\hat{\boldsymbol{y}} + \frac{1}{3}(1+2S)\,\hat{\boldsymbol{z}}\hat{\boldsymbol{z}}\right) - \frac{1}{2}\mathbb{1} \\
&= \begin{pmatrix} -\frac{S}{2} & 0 & 0 \\ 0 & -\frac{S}{2} & 0 \\ 0 & 0 & S \end{pmatrix},
\end{aligned} \tag{7.3}$$

where we recover the tensor form of $\boldsymbol{Q}$ from Eq. (3.4). Similarly, the polar vector order parameter is given by

$$\begin{aligned}
\boldsymbol{P} &= \langle \boldsymbol{m}_1 \rangle = \sum_{i,j\in\{x,y,z\}} \left(\psi_{i,j} - \psi_{i,-j}\right)\hat{\boldsymbol{j}} \\
&= \Big(\left(\psi_{y,x} - \psi_{y,-x} + \psi_{z,x} - \psi_{z,-x}\right)\hat{\boldsymbol{x}} + \left(\psi_{x,y} - \psi_{x,-y} + \psi_{z,y} - \psi_{z,-y}\right)\hat{\boldsymbol{y}} \\
&\quad + \left(\psi_{x,z} - \psi_{x,-z} + \psi_{y,z} - \psi_{y,-z}\right)\hat{\boldsymbol{z}}\Big) \\
&= \frac{1}{12}\left((2\alpha + 2\gamma)\,\hat{\boldsymbol{x}} + 0\,\hat{\boldsymbol{y}} + 0\,\hat{\boldsymbol{z}}\right) \\
&= \begin{pmatrix} \frac{1}{6}(\alpha+\gamma) \\ 0 \\ 0 \end{pmatrix}.
\end{aligned} \tag{7.4}$$

Lastly, we can calculate the biaxial order parameter as

$$\begin{aligned}\boldsymbol{\Delta} &= \frac{3}{2}\left\langle \boldsymbol{m}_3^2 - \frac{1}{3}\mathbb{1}\right\rangle = \sum_{i,j\neq k}\frac{3}{2}\left(\psi_{i,j} + \psi_{i,-j}\right)\hat{\boldsymbol{k}}\hat{\boldsymbol{k}} - \frac{1}{2}\mathbb{1} \\ &= \frac{3}{2}\Big(\left(\psi_{y,z} + \psi_{y,-z} + \psi_{z,y} + \psi_{z,-y}\right)\hat{\boldsymbol{x}}\hat{\boldsymbol{x}} + \left(\psi_{x,z} + \psi_{x,-z} + \psi_{z,x} + \psi_{y,-z}\right)\hat{\boldsymbol{y}}\hat{\boldsymbol{y}} \\ &\quad + \left(\psi_{z,x} + \psi_{z,-x} + \psi_{z,y} + \psi_{z,-y}\right)\hat{\boldsymbol{z}}\hat{\boldsymbol{z}}\Big) - \frac{1}{2}\mathbb{1} \\ &= \frac{1}{4}\begin{pmatrix} S-\alpha'-\gamma' & 0 & 0 \\ 0 & S+\alpha'-\beta' & 0 \\ 0 & 0 & -2S+\beta'+\gamma' \end{pmatrix}. \end{aligned} \tag{7.5}$$

This provides a way to compare order parameters and describe them as a function of the parameters $S, \alpha, \alpha', \beta', \gamma, \gamma'$.

The orientation distribution function can also be inserted into the free energy functional Eq. (4.15). When the excluded volume of two particles is known, the free energy can be minimized with respect to the different parameters. The solutions provide insight in the different phases that the liquid crystal exhibits and the types of phase transitions that are present. However, the large number of parameters makes this approach more complicated. In the remained of this chapter, a more systematic method will be introduced based on representation theory and symmetry arguments.

7.4 A basis of symmetry-adapted functions

Unfortunately, the eigenvectors of the 12×12 excluded volume matrix in Eq. (7.1) are too complicated to work with, let alone interpret. In this section, we will determine a complete set of functions that can act as a basis of the excluded volume. The two ingredients needed are symmetry arguments and the irreducible representations of O_h. Let us first take a look at the symmetries of the excluded volume.

First of all, the excluded volume has a global symmetry, which means that applying the same symmetry operation $p \in O_h$ to two particles with orientations A and B leaves the excluded volume invariant. The global symmetry is equal to the symmetry of a cube and is therefore described by the O_h group. A result of the global symmetry is that the excluded volume only depends on the relative orientation of the particles, i.e. $\mathcal{E}(p_1 A, p_2 A) = \mathcal{E}(A, p_1^{-1} p_2\, A) = E(p_{12})$. The second symmetry is interchange symmetry, since interchanging the two particles does not change the excluded volume. Thirdly, the excluded volume is invariant under inversion of the symmetry operation, which means that applying p to the first particle and applying p^{-1} to the second particle are equivalent with respect to the excluded volume. The last symmetry of the excluded volume can be attributed to the internal symmetry of the particles. In the case of banana-shaped particles, this symmetry is described by the C_{2v} point group. Applying one of the four symmetry operations $h \in C_{2v}$ to a banana-shaped particle leaves the excluded volume invariant. Thus, the excluded volume of two particles with orientation A and B respectively has the following symmetries:

1. global symmetry: $\mathcal{E}(pA, pB) = \mathcal{E}(A, B)$;
2. interchange symmetry: $\mathcal{E}(A, B) = \mathcal{E}(B, A)$;
3. inversion symmetry: $\mathcal{E}(A, pB) = \mathcal{E}(p^{-1}A, B)$;
4. internal symmetry: $\mathcal{E}(h_1\, p\, h_2\, A, B) = \mathcal{E}(pA, B)$.

The next step is determining the complete set of functions that fully describe the symmetry of the excluded volume. The irreducible representations of O_h provide us with such a complete set of functions for an object with O_h symmetry. Since that is one of the symmetries of the excluded volume, the irreducible representations of O_h can be used as a starting point. The irreducible representations of O_h can be determined with the irreducible representations of O and the fact that $O_h = O \times Z_2$. The result can be written as ten matrices with matrix elements $Q^{\lambda}_{i,j}(p)$, where λ labels the ten irreducible matrices, and i and j label the matrix elements. The size of the matrix depends on the dimensionality of the irreducible representation. A one-dimensional representation is represented by a 1×1 matrix, a two-dimensional representation by a 2×2 matrix, and a three-dimensional representation by a 3×3 matrix. The value of each matrix element depends on the symmetry operation p. In this step, the global symmetry and the interchange symmetry are included.

Now, let us implement the inversion and internal symmetry of the excluded volume into our representation theory framework. This is possible by averaging over the elements of C_{2v} and the elements of O_h and their inverse. The matrix elements of the resulting symmetry-adapted functions $\bar{Q}^{\lambda}(p)$ are given by

$$\bar{Q}^{\lambda}_{ij}(p) = \frac{1}{2|C_{2v}|^2} \sum_{q \in \{p, p^{-1}\}} \sum_{h \in C_{2v}} \sum_{h' \in C_{2v}} Q^{\lambda}_{im}(h) Q^{\lambda}_{mn}(q) Q^{\lambda}_{nj}(h'), \tag{7.6}$$

where the number of elements of C_{2v} is $|C_{2v}| = 4$. Instead of writing the symmetry-adapted functions as matrices, we can represent each matrix element $\bar{Q}^{\lambda}_{ij}$ as a vector of 48 elements with a value for each symmetry operation $p \in O_h$. This gives a total of 48 functions or vectors with 48 elements. The averaging reduces the number of independent functions from a maximum of 48 to 7. These seven functions form a basis of the excluded volume and fully describe the symmetry properties of the excluded volume.

Lastly, we can reduce the number of symmetry operations needed to describe the symmetry of the excluded volume from 48 to 12. In this way, the twelve symmetry operations $\bar{p}$ correspond to the twelve distinguishable orientations, or equivalently, to one element out of each coset $\gamma \in \Gamma$. This reduces the size of our calculation from 7 vectors of 48 elements to 7 vectors of 12 elements. These independent (unnormalized) functions v_i are given by

$$v_1 = \begin{pmatrix} 1 \\ 1 \\ 1 \\ 1 \\ 1 \\ 1 \\ 1 \\ 1 \\ 1 \\ 1 \\ 1 \\ 1 \end{pmatrix}, v_2 = \begin{pmatrix} 1 \\ -1 \\ -1 \\ 1 \\ 1 \\ -1 \\ -1 \\ -1 \\ 1 \\ 1 \\ -1 \\ 1 \end{pmatrix}, v_3 = \begin{pmatrix} 2 \\ -2 \\ 0 \\ -1 \\ -1 \\ 2 \\ 0 \\ 2 \\ -1 \\ -1 \\ -2 \\ 2 \end{pmatrix}, v_4 = \begin{pmatrix} -2 \\ -5 \\ 7 \\ 1 \\ 1 \\ -2 \\ 7 \\ -2 \\ 1 \\ 1 \\ -5 \\ -2 \end{pmatrix}, v_5 = \begin{pmatrix} 2 \\ 1 \\ 1 \\ -1 \\ -1 \\ -2 \\ 1 \\ -2 \\ -1 \\ -1 \\ 1 \\ 2 \end{pmatrix}, v_6 = \begin{pmatrix} 2 \\ -1 \\ 0 \\ 0 \\ 0 \\ 0 \\ 0 \\ 0 \\ 0 \\ 0 \\ 1 \\ -2 \end{pmatrix}, v_7 = \begin{pmatrix} 1 \\ 2 \\ 0 \\ 0 \\ 0 \\ 0 \\ 0 \\ 0 \\ 0 \\ 0 \\ -2 \\ -1 \end{pmatrix}. \tag{7.7}$$

These functions can be used in the expansion of the orientation distribution function as well as the expansion of the excluded volume

$$\mathcal{E}(\bar{p}) = \sum_{i=1}^{7} c_i v_i(\bar{p}), \tag{7.8}$$

with c_i the expansion coefficients. Instead of twelve complicated eigenvectors that are degenerate, we now have a set of seven vectors that fully describe the excluded volume. Except for the first eigenvector v_1, these functions are not seven of the twelve eigenvectors of the 12×12 matrix in Eq. (7.1) because these functions and the eigenvectors are written in a different basis. Since the basis transformation between these two quantities is not known, they cannot be linked one-to-one.

7.5 The overlap function

To determine the expansion coefficients, we need seven expressions for the seven different excluded volumes. Due to the fact that the excluded volume is difficult to determine for banana-shaped particles because of their non-convex shape, we will be considering an easier version of C_{2v}-symmetric particles. Namely, a combination of two cuboids in a T-shape (like one of the Tetris shapes), which we will call boomies (see Fig. 7.2).

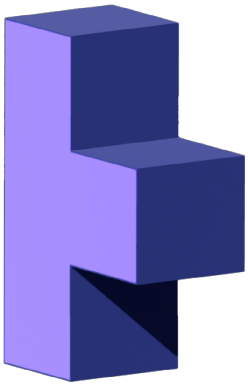

Figure 7.2: An example of a boomy: a particle that is composed of two rigidly-connect cuboids.

We are looking for an analytic expression of the overlap function. By integrating this overlap function over the whole space, the excluded volume of two boomies can be obtained. This allows us to fix the expansion coefficients c_i and brings us a step closer towards a description of the excluded volume.

First, consider two cuboids A and B in the same orientation with their axes aligned with the coordinate frame. Their dimensions in the x, y, and z-direction are $\boldsymbol{a} = a_1, a_2, a_3$ and $\boldsymbol{b} = b_1, b_2, b_3$. The diameters of the two cuboids overlapping is then defined as $d_k = \frac{1}{2}(a_k + b_k)$ for $k = 1, 2, 3$. The overlap function $\bar{\chi}^{AB}(\boldsymbol{r})$ is simply a product of Heaviside step functions

$$\chi^{AB}(\boldsymbol{r}, \boldsymbol{d}) = \prod_{k=1}^{3} \theta(d_k - |r_k|) = \prod_{k=1}^{3} \theta(d_k - r_k)\,\theta(d_k + r_k), \tag{7.9}$$

where $\boldsymbol{r} = (r_1, r_2, r_3)$ is the distance between the centers of the two cuboids. This overlap function gives 1 if the two bodies overlap and 0 if they do not. We can also introduce the non-overlap function $\bar{\chi}^{AB}(\boldsymbol{r}) = 1 - \chi^{AB}(\boldsymbol{r})$, which is equal to 0 if the particles overlap and 1 if the particles do not overlap.

We want the overlap function to depend on the rotation of the two particles. Since the excluded volume only depends on the relative orientation of two particles, we can keep the orientation of one cuboid fixed and apply one of the twelve symmetry operations to the other cuboid. The new dimensions of the second particle can be obtained by multiplying the matrix $\boldsymbol{R}(\bar{p})$ corresponding to that symmetry operation $\bar{p}$ with the vector $\boldsymbol{b}$ of the three dimensions of the second particle, such that we get the new dimensions

$$\boldsymbol{b}'(\bar{p}) = \boldsymbol{R}(\bar{p})\,\boldsymbol{b}. \tag{7.10}$$

Calculating the new diameters gives $d'_k = \frac{1}{2}(a_k + b'_k)$ for $k = 1, 2, 3$. These can be used to calculate the overlap function from Eq. (7.9).

Consider now two bodies A and B that are composed of two rigidly-connected cuboids X and Y, such that $A = A_X \cup A_Y$ and $B = B_X \cup B_Y$. A cuboid of one particle can only overlap with none, one or both of the cuboids of the other particle, but not with the other cuboid of the same particle. The dimensions of X are $\boldsymbol{x} = (x_1, x_2, x_3)$, and the dimensions of Y are $\boldsymbol{y} = (y_1, y_2, y_3)$. Similar to the previous example, we keep the orientation of the two cuboids in A fixed and apply the twelve symmetry operations $\bar{p}$ to both cuboids of B. The dimensions of B_X and B_Y then become

$$\boldsymbol{x}'(\bar{p}) = \boldsymbol{R}(\bar{p})\,\boldsymbol{x}, \tag{7.11}$$
$$\boldsymbol{y}'(\bar{p}) = \boldsymbol{R}(\bar{p})\,\boldsymbol{y}. \tag{7.12}$$

Place A in the orientation Z_x with A_X on the left of A_Y with the vector $(1, 0, 0)$ connecting the two cuboids. If we now define the origin of our coordinate frame to be in the center of A_X, the distances between the four cuboids are given by

$$\begin{aligned}
\boldsymbol{r}^{11} &\equiv \boldsymbol{r}^{A_X,B_X} = \boldsymbol{r}, \\
\boldsymbol{r}^{12} &\equiv \boldsymbol{r}^{A_X,B_y} = \boldsymbol{r} + d^{A_X,A_Y}\,\boldsymbol{R}(\bar{p})\,(1,0,0)^T, \\
\boldsymbol{r}^{21} &\equiv \boldsymbol{r}^{A_Y,B_X} = \boldsymbol{r} - d^{A_X,A_Y}\,(1,0,0)^T, \\
\boldsymbol{r}^{22} &\equiv \boldsymbol{r}^{A_Y,B_Y} = \boldsymbol{r} + d^{A_X,A_Y}\,\boldsymbol{R}(\bar{p})\,(1,0,0)^T - d_{A_X,A_Y}\,(1,0,0)^T,
\end{aligned} \tag{7.13}$$

where $d_k^{A_X,A_Y} = \frac{1}{2}(x_k + y_k)$, and $X \Leftrightarrow 1$ and $Y \Leftrightarrow 2$ to make the expression more readable. The diameters of the overlap of the four cuboids are given by

$$\begin{aligned}
d_k^{11} &= \frac{1}{2}(x_k + x'_k), \\
d_k^{12} &= \frac{1}{2}(x_k + y'_k), \\
d_k^{21} &= \frac{1}{2}(y_k + x'_k), \\
d_k^{22} &= \frac{1}{2}(y_k + y'_k).
\end{aligned} \tag{7.14}$$

In writing down the overlap function, we can distinguish six cases:

1. none of the cuboids overlap,
2. one cuboid of particle A overlaps with one cuboid of particle B or vice versa,
3. the same as case 2, but now the other cuboid of particle A overlaps with the other cuboid of particle B,
4. one cuboid of particle A overlaps with both cuboids of particle B or vice versa,

5. the same as case 4, but now the other cuboid of particle A overlaps with one of the cuboids of particle B,

6. both cuboids of particle A overlap with both cuboids of particle B.

When writing each of these cases as a product of overlap functions χ and non-overlap functions $\bar{\chi}$, they all give one or more contributions to the total overlap function. Only one of the terms however, namely the term that corresponds to the physical situation of overlap between the cuboids, is non-zero. The total overlap function is therefore a sum over all appropriate contributions given in Table 7.3, where $\chi^{ij} \equiv \chi(\boldsymbol{r}^{ij}, \boldsymbol{d}^{ij})$, with $i, j = 1, 2$. There are $0 + 4 + 2 + 4 + 4 + 1 = 15$ terms in total. Case 1 does not contribute a term to the total overlap function since it is a product of non-overlap functions and therefore always returns zero whenever the two particles overlap.

Table 7.3

Case	Contributions
1	0
2	$\chi^{11}\bar{\chi}^{12}\bar{\chi}^{21}\bar{\chi}^{22} + \bar{\chi}^{11}\chi^{12}\bar{\chi}^{21}\bar{\chi}^{22} + \bar{\chi}^{11}\bar{\chi}^{12}\chi^{21}\bar{\chi}^{22} + \bar{\chi}^{11}\bar{\chi}^{12}\bar{\chi}^{21}\chi^{22}$
3	$\chi^{11}\bar{\chi}^{12}\bar{\chi}^{21}\chi^{22} + \bar{\chi}^{11}\chi^{12}\chi^{21}\bar{\chi}^{22}$
4	$\chi^{11}\chi^{12}\bar{\chi}^{21}\bar{\chi}^{22} + \chi^{11}\bar{\chi}^{12}\chi^{21}\bar{\chi}^{22} + \bar{\chi}^{11}\chi^{12}\bar{\chi}^{21}\chi^{22} + \bar{\chi}^{11}\bar{\chi}^{12}\chi^{21}\chi^{22}$
5	$\chi^{11}\chi^{12}\chi^{21}\bar{\chi}^{22} + \chi^{11}\chi^{12}\bar{\chi}^{21}\chi^{22} + \chi^{11}\chi^{12}\chi^{21}\chi^{22} + \chi^{11}\chi^{12}\chi^{21}\chi^{22}$
6	$\chi^{11}\chi^{12}\chi^{21}\chi^{22}$

These overlap terms are all dependent on the symmetry operation applied to the second particle via the diameter $\boldsymbol{d}$. In principle, the excluded volume can be calculated from the overlap function by integrating over the whole space

$$\mathcal{E}(\bar{p}, \bar{p}') = \int d\boldsymbol{r}_1 \int d\boldsymbol{r}_2 \, \chi(\boldsymbol{r}^{ij}, \boldsymbol{d}^{ij}). \tag{7.15}$$

Since the excluded volume only depends on the relative orientation, we can write $\mathcal{E}(\bar{p}, \bar{p}') = E(\bar{p})$ and obtain twelve expressions for the excluded volume of two boomies as a function of the dimensions of the particles and the relative orientation. Using these expressions together with the expansion of the excluded volume in the seven symmetry-adapted functions, the seven expansion coefficients can be determined. That would bring us a step further towards our goal of a microscopic description of a liquid-crystal of banana-shaped particles and its phases and phase transitions. Unfortunately, calculating $\mathcal{E}(\bar{p}, \bar{p}')$ via this way analytically has not yet been achieved.

Summary, conclusions, and outlook

In Chapter 1, we started with an introduction to the topic of liquid crystals. We looked at the different phases of a system of rod-like particles, such as the nematic and smectic liquid crystal phases. We also discussed the difference between thermotropic and lyotropic liquid crystals. Since the particles we have considered in this thesis are colloidal, the resulting liquid crystals are lyotropic, i.e. the phase transitions occur as a function of density. Additionally, a range of different particle shapes and their symmetries were discussed.

The focus of this thesis was on liquid crystals of one of those particle shapes, namely bent-core or banana-shaped particles. Their properties were discussed in Chapter 2. Liquid crystals of banana-shaped particles were observed, both in theory, experiments and simulations, to exhibit additional phases such as the twist-bend and splay-bend phases due to coupling between the nematic director and the polar order. The mechanism behind this coupling was identified to be the bend flexoelectric effect which resulted in induced bend deformations in the nematic director, combined with a twist or splay distortion to enable extension in three dimensions. After destabilizing the smectic phase by introducing a polydisperse distribution of particle lengths or by introducing curvature in the particle shape, the twist-bend and splay-bend phases were observed in computer simulations in 2019 and a year later in experiments. Furthermore, the twist-splay-bend phase was postulated following its observation in simulations to be an intermediate phase between the twist-bend phase and the splay-bend phase.

In Chapter 3, the first theoretical model of a liquid crystal was discussed. This theory is known as Landau-de Gennes theory and based on the Landau theory of phase transitions. By considering the grand potential instead of the free energy and writing it as an expansion in the nematic tensor order parameter $\boldsymbol{Q}$, the isotropic to nematic phase transition could be studied. After including the polar vector order parameter $\boldsymbol{P}$ to describe the coupling between the nematic director and the polar order, numerical values were found for the elastic constants K_{11} and K_{22} for which a nematic to twist-bend or a nematic to splay-bend phase transition occurred. By varying the expansion coefficient l_3, the twist-bend to splay-bend and splay-bend to twist-bend transitions could be reproduced. However, Landau-de Gennes does have some shortcomings. As a phenomenological theory, any microscopic information needs to be included manually or by fitting it to other theoretical, experimental or simulation results. Defining the right order parameters and proving that the relevant invariants are included is also not trivial.

Therefore, an alternative to Landau-de Gennes theory was proposed in Chapter 4, namely density functional theory. Density function theory was introduced as a microscopic approach based on the idea that the free energy can be written as a functional of the one-particle distribution. The properties of the constituting particles were contained in the Mayer or overlap function, or in the case of spatially homogeneous phases, in the excluded volume. Bifurcation analysis then provided a way to study what happens near a symmetry-breaking phase transition. We found that the problem of solving the first bifurcation equation could be reduced to determining the eigenvalues and eigenvectors of the excluded volume. Unfortunately, an analytical expression for the excluded volume does not exist because of the non-convex shape of banana-shaped

particles. However, symmetry arguments can be used to describe the excluded volume of two banana-shaped particles. Therefore, Chapter 5 included an introduction to point groups, cosets and representation theory needed to study the symmetries of the excluded volume. The point groups describing the symmetry of a cube and a banana-shaped were identified to be O_h and C_{2v} and their elements were listed.

In Chapter 6 a simple model of a liquid-crystal of hard rod-like particles was studied. The first approach was based on the Zwanzig model of rods with restricted orientations, where the free energy could be written as an expansion in the density. By defining a scalar order parameter S, we determined the values of S that minimized the free energy at a given density. In this way, the stability of the isotropic and nematic phase could be investigated, as well as the isotropic-nematic coexistence. Next, we performed bifurcation analysis on a liquid crystal of rods with restricted orientations by both determining the eigenvalues and eigenvectors of the excluded volume directly, as well as using the set of irreducible representations of the symmetry group C_3 as a basis of the excluded volume of two rods. Both methods succeeded in describing the isotropic and nematic phase, but with the latter we were also able to find the bifurcation density and make a connection to Landau theory. Next, we studied a system of aligned rods with smectic order by writing the Mayer function as a product of theta functions and calculating its Fourier transform. The instability in the density could then be studies by calculating for which density $\rho\hat{f}(\boldsymbol{q}) \to 1$. In this way, we were able to determine the packing fraction above which a smectic phase would be stable and the nature of the nematic to smectic phase transition, namely continuous.

In Chapter 7, we combined everything we had learned so far and applied it to a liquid crystal of banana-shaped particles with restricted orientations. We identified twelve distinguishable orientations of a banana-shaped particle and linked them to the 24 rotations that leave a cube invariant. We showed that two particles, both in one of the twelve orientations, lead to a 12×12 matrix with seven different excluded volumes. Unfortunately, the eigenvectors of this matrix were considered too complicated to work with. We showed how symmetries of the orientation distribution function can be manually broken by introducing parameters that are nonzero if the symmetry is broken. Inserting this orientation distribution function into the free energy provided a way to minimize the free energy with respect to these parameters and recover liquid crystal phases and the regimes where they are stable. We were also able to write down explicit expressions of the tensor and vector order parameters.

However, the most promising result was finding a basis of symmetry-adapted functions that described the full symmetry of the excluded volume, including the global symmetry, interchange symmetry, inversion symmetry and internal symmetry of the particles. These seven functions indicated that the excluded volume had seven degrees of freedom, which agreed with our earlier result of seven different excluded volumes. In order to expand the excluded volume in terms of these functions, the expansion coefficients needed to be determined. We were able to write down an analytic expression of the overlap function of two boomies, which are particles with the same C_{2v} symmetry as banana-shaped particles for which the overlap function can be more easily written down. However, further research is needed to integrate out the spatial dependence of the overlap function such that the excluded volume is recovered for different orientations of the particles. That would allow the expansion coefficients to be determined, which is the last ingredient needed to perform bifurcation analysis.

My first recommendation for further research is therefore to perform bifurcation analysis on a system of C_{2v}-symmetric particles with restricted orientations. With the complete set of functions describing the excluded volume and the expansion coefficients, one is able to determine the bifurcation density and what phases become stable at which densities. However, the system that we have studied in this thesis is nothing more than a simple toy model. It only allows

for orientations that align with the axes of the coordinate frame, which means that it can only predict simple phases such as an isotropic-like phase and a nematic phase. In order to describe more complicated phases like the twist-bend phase and smectic phases such as the splay-bend phase, one needs to allow for continuous orientations and spatial modulations. Continuous orientations can be implemented by going from discrete point groups to continuous groups. This means replacing irreducible representations that represent the symmetry of a point group by Wigner matrices [45, 46] that describe the symmetry of continuous groups, like is done in Ref. [47] for rectangular slabs with D_{2h} symmetry. Implementing spatial modulations is more complicated, since it involves calculating the Fourier transform of the Mayer function, similar to what is described in Section 6.3. The Mayer function describing the overlap of two boomies has a lot more terms than the Mayer function for rods. The condition for an instability in the density would therefore be a lot more difficult to interpret.

The systematic and microscopic approach towards describing liquid crystals as discussed in Chapter 7 can easily be extended to different particle shapes. By replacing the point group C_{2v} with the corresponding point group describing the symmetry of the new particle, one would find a different set of symmetry-adapted functions. By calculating the overlap function of a particle with that symmetry, one would be able to determine the expansion coefficients and perform bifurcation analysis in the same way as described above.

Lastly, although Landau-de Gennes theory has some drawbacks, it is less complicated than density functional theory. As discussed in Chapter 3, the Landau coefficients and elastic constants were found by fitting them to results from Onsager theory. This was sufficient to describe the twist-bend and splay-bend phases, but did not succeed in describing the intermediate twist-splay-bend phase. However, this could be because we were looking in the wrong regime of expansion coefficients. An opportunity lies in fitting the coefficients to results from simulations that did reproduce the intermediate twist-splay-bend phase. These results could be used to theoretically confirm the existence of the intermediate twist-splay-bend phase.

Bibliography

[1] H. Kawamoto, "The history of liquid-crystal displays", *Proceedings of the IEEE* **90**, 460–500 (2002).

[2] M. Mitov, "Liquid-Crystal Science from 1888 to 1922: Building a Revolution", *ChemPhysChem* **15**, 1245–1250 (2014).

[3] P. de Gennes, "Fluctuations d'orientation et diffusion Rayleigh dans un cristal nématique", *Comptes rendus de l'Académie des Sciences B* **266**, 15–17 (1968).

[4] L. Onsager, "The Effects of Shape on the Interaction of Colloidal Particles", *Annals of the New York Academy of Sciences* **51**, 627–659 (1949).

[5] M. Chiappini, T. Drwenski, R. van Roij and M. Dijkstra, "Biaxial, Twist-bend, and Splay-bend Nematic Phases of Banana-shaped Particles Revealed by Lifting the "Smectic Blanket"", *Physical Review Letters* **123**, 068001 (2019).

[6] C. Fernández-Rico, M. Chiappini, T. Yanagishima, H. de Sousa, D. G. Aarts, M. Dijkstra and R. P. Dullens, "Shaping colloidal bananas to reveal biaxial, splay-bend nematic, and smectic phases", *Science* **369** (2020).

[7] P.-G. de Gennes and J. Prost, "The physics of liquid crystals" (Oxford University Press, 1993).

[8] G. Vertogen and W. H. de Jeu, "Thermotropic Liquid Crystals, Fundamentals" (Springer-Verlag, 1988).

[9] C. W. Oseen, "The theory of liquid crystals", *Transactions of the Faraday Society* **29**, 883–899 (1933).

[10] F. C. Frank, "I. Liquid crystals. On the theory of liquid crystals", *Discussions of the Faraday Society* **25**, 19–28 (1958).

[11] Z. Kos, J. Aplinc, U. Mur and M. Ravnik, "Mesoscopic Approach to Nematic Fluids", 51–93 (2019).

[12] A. M. F. Neto and S. R. Salinas, "The Physics of Lyotropic Liquid Crystals: Phase Transitions and Structural Properties" (Oxford University Press, 2005).

[13] J. Xu and J. Z. Chen, "General liquid-crystal theory for anisotropically shaped molecules: Symmetry, orientational order parameters, and system free energy", *Physical Review E* **102**, 062701 (2020).

[14] A. Jákli, O. D. Lavrentovich and J. V. Selinger, "Physics of liquid crystals of bent-shaped molecules", *Reviews of Modern Physics* **90**, 045004 (2018).

[15] C. Anzivino, R. van Roij and M. Dijkstra, "A Landau-de Gennes theory for twist-bend and splay-bend nematic phases of colloidal suspensions of bent rods", *The Journal of Chemical Physics* **152**, 224502 (2020).

[16] R. B. Meyer, "Piezoelectric effects in liquid crystals", *Physical Review Letters* **22**, 918 (1969).

[17] M. Chiappini, "Nematics that splay, twist, and bend: Understanding periodically modulated liquid crystal phases and their structural and dynamical properties", PhD thesis (Utrecht University, 2020).

[18] D. Chen, M. Nakata, R. Shao, M. R. Tuchband, M. Shuai, U. Baumeister, W. Weissflog, D. M. Walba, M. A. Glaser, J. E. Maclennan et al., "Twist-bend heliconical chiral nematic liquid crystal phase of an achiral rigid bent-core mesogen", *Physical Review E* **89**, 022506 (2014).

[19] M. Chiappini and M. Dijkstra, "A generalized density-modulated twist-splay-bend phase of banana-shaped particles", *Nature Communications* **12**, 2157 (2021).

[20] L. D. Landau, "On the theory of phase transitions. I.", *Journal of Experimental and Theoretical Physics* **11**, 19 (1937).

[21] D. Andrienko, "Introduction to liquid crystals", *Journal of Molecular Liquids* **267**, 520–541 (2018).

[22] J. C. Everts, M. T. J. J. M. Punter, S. Samin, P. van der Schoot and R. van Roij, "A Landau-de Gennes theory for hard colloidal rods: Defects and tactoids", *The Journal of Chemical Physics* **144**, 194901 (2016).

[23] R. van Roij, "The isotropic and nematic liquid crystal phase of colloidal rods", *European Journal of Physics* **26**, S57–S67 (2005).

[24] S. Wolfsheimer, C. Tanase, K. Shundyak, R. van Roij and T. Schilling, "Isotropic-nematic interface in suspensions of hard rods: Mean-field properties and capillary waves", *Physical Review E* **73**, 061703 (2006).

[25] I. Dozov, "On the spontaneous symmetry breaking in the mesophases of achiral banana-shaped molecules", *Europhysics Letters* **56**, 247 (2001).

[26] S. Dhakal and J. V. Selinger, "Statistical mechanics of splay flexoelectricity in nematic liquid crystals", *Physical Review E* **81**, 031704 (2010).

[27] S. M. Shamid, S. Dhakal and J. V. Selinger, "Statistical mechanics of bend flexoelectricity and the twist-bend phase in bent-core liquid crystals", *Physical Review E* **87**, 052503 (2013).

[28] Z. Parsouzi, S. M. Shamid, V. Borshch, P. K. Challa, A. R. Baldwin, M. G. Tamba, C Welch, G. H. Mehl, J. T. Gleeson, A. Jakli, O. D. Lavrentovich, D. W. Allender, J. V. Selinger and S. Sprunt, "Fluctuation Modes of a Twist-Bend Nematic Liquid Crystal", *Physical Review X* **6**, 021041 (2016).

[29] C. Anzivino, R. Van Roij and M. Dijkstra, "Coupling between splay deformations and density modulations in splay-bend phases of bent colloidal rods", *Physical Review E* **105**, L022701 (2022).

[30] S. S. Turzi, "On the Cartesian definition of orientational order parameters", *Journal of Mathematical Physics* **52**, 053517 (2011).

[31] R. Evans, "The nature of the liquid-vapour interface and other topics in the statistical mechanics of non-uniform, classical fluids", *Advances in Physics* **28**, 143–200 (1979).

[32] R. F. Kayser and H. J. Raveché, "Bifurcation in Onsager's model of the isotropic-nematic transition", *Physical Review A* **17**, 2067–2072 (1978).

[33] B. Mulder, "Density-functional approach to smectic order in an aligned hard-rod fluid", *Physical Review A* **35**, 3095–3101 (1987).

[34] B. M. Mulder, "Bifurcation Analysis of Liquid Crystal Phase Transitions", from `http://arxiv.org/abs/1806.11018` (2018).

[35] R. Zwanzig, "First-Order Phase Transition in a Gas of Long Thin Rods", *The Journal of Chemical Physics* **39**, 1714–1721 (1963).

[36] G. Vroege and H. Lekkerkerker, "Phase transitions in lyotropic colloidal and polymer liquid crystals", *Reports on Progress in Physics* **55**, 1241 (1992).

[37] F Bisi and R Rosso, "Excluded-volume potential for rigid molecules endowed with C2v symmetry", *European Journal of Applied Mathematics* **23**, 29–60 (2012).

[38] M. S. Dresselhaus, G. Dresselhaus and A. Jorio, "Applications of group theory to the physics of solids" (Springer New York, 2006).

[39] M. Lax, "Symmetry principles in solid state and molecular physics" (Courier Corporation, 2001).

[40] D. Perkins, "10 Crystal morphology and symmetry", *University of North Dakota*, from `https://opengeology.org/Mineralogy/10-crystal-morphology-and-symmetry/`.

[41] Q. Westrich, "Young's Natural Representations of $\mathcal{S}_4$", from `https://arxiv.org/abs/1112.0687` (2011).

[42] M. Chaplin, "Molecular orbitals for water (H_2O)", from `https://water.lsbu.ac.uk/water/h2o_orbitals.html` (2021).

[43] R. Van Roij, M. Dijkstra and R. Evans, "Interfaces, wetting, and capillary nematization of a hard-rod fluid: Theory for the Zwanzig model", *The Journal of Chemical Physics* **113**, 7689–7701 (2000).

[44] L. S. Ornstein and F. Zernike, "Accidental deviations of density and opalescence at the critical point of a single substance", *Proceedings of the Section of Sciences* **17**, 793 (1914).

[45] D. M. Brink and G. R. Satchler, "Angular Momentum" (Clarendon Press, 1968).

[46] M. A. Morrison and G. A. Parker, "A Guide to Rotations in Quantum Mechanics", *Australian Journal of Physics* **40**, 465–498 (1987).

[47] B. Mulder, "Isotropic-symmetry-breaking bifurcations in a class of liquid-crystal models", *Physical Review A* **39**, 360–370 (1989).